Fuel 371 (2024) 131897

Contents lists available at ScienceDirect

Fuel

journal homepage: www.elsevier.com/locate/fuel

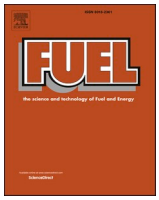

Analysis of the performance of kinetic reaction mechanisms in estimating N_2O mole fractions in 70/30 vol% NH_3/H_2 premixed flames

A. Alnasif [a,b,*], J. Jójka [c], S. Mashruk [a], T. Nagy [d], A. Valera-Medina [a]

[a] College of Physical Sciences and Engineering, Cardiff University, Queen's Buildings, Cardiff CF24 3AA, United Kingdom
[b] Engineering Technical College of Al-Najaf, Al-Furat Al-Awsat Technical University, Najaf 31001, Iraq
[c] Institute of Thermal Engineering, Poznan University of Technology, 60-965 Poznan, Poland
[d] Institute of Materials and Environmental Chemistry, Research Centre for Natural Sciences, 1117 Budapest, Hungary

ARTICLE INFO

Keywords:
Kinetic reaction mechanism
Ammonia
Burner stabilised-stagnation flow
Kinetic modelling
N_2O mole fraction

ABSTRACT

To address the environmental concerns associated with fossil fuels, this study explores ammonia (NH_3) blended with hydrogen (H_2) as an alternative fuel. While offering reduced CO_2 emissions and leveraging existing infrastructure, NH_3-H_2 combustion notably leads to the production of nitrogen oxides (NOx), including the greenhouse gas nitrous oxide (N_2O). Understanding the flame structure and chemistry responsible for N_2O formation and consumption is crucial. This study comprehensively investigates various kinetic reaction mechanisms, focusing on accurately estimating N_2O mole fractions and identifying mechanisms that align closely with experimental data. Sixty-seven chemical kinetic mechanisms have been numerically analysed across various equivalence ratios (φ) ranging from 0.57 to 1.4, utilizing the Premixed Stagnation Flame Model via Chemkin-Pro software. Simulations in a Perfectly Stirred Reactor were also conducted for the kinetic models that demonstrated high accuracy within the burner-stabilized stagnation flame model and closely matched experimental measurements with minimal discrepancies. This was done to determine whether the tested models, which perform accurately, maintain their performance across different combustion configurations. A preliminary assessment was carried out using the Normalized Error Approach, taking into account the uncertainty of experimental measurements, to compare the numerical results with experimental data. This method is significant in determining whether the discrepancies between the model's calculations and the experimental results, considering the experimental uncertainties, are within an acceptable range of error. The sensitivity analysis along with rate of production/consumption of N_2O investigation at several conditions of equivalence ratio (0.6,1,1.4) has been conducted to check the discrepancies among the mechanisms and shed light on the reactions that dominate the formation/consumption of N_2O at different conditions. The study revealed that the kinetic model developed by Klippenstein et al. (2018) demonstrates remarkable accuracy in predicting N_2O mole fractions across a range of conditions, specifically within the equivalence ratio range of 0.6 to 1.4. In this range, the normalised error values were observed to be less than 1, signifying that the experimental values align closely with the numerical expectations, considering the uncertainty. However, it is noteworthy that the model's accuracy appears to decrease in lean flame scenarios, particularly when the equivalence ratio falls between 0.57 and 0.585. In these conditions, higher normalised error values exceeding 1 were recorded, suggesting a possible deviation between numerical predictions and experimental observations. Along with that the rate of production/consumption analysis revealed the $NH + NO \rightleftharpoons N_2O + H$ reaction has a dominant role in the formation of N_2O for all studied conditions, while the consumption of N_2O is dominated by reactions $N_2O + H \rightleftharpoons N_2 + OH$ and $N_2O (+M) \rightleftharpoons N_2 + O (+M)$ at all investigated conditions.

1. Introduction

The vast spreading population and rapid economic development in recent decades have affected dramatically the global energy consumption. Fossil fuel sources such as coal, petroleum and natural gas are kept at the top of the major energy sources across the world. The emissions

* Corresponding author at: College of Physical Sciences and Engineering, Cardiff University, Queen's Building, Cardiff CF24 3AA, United Kingdom.
E-mail address: AlnasifAH@cardiff.ac.uk (A. Alnasif).

https://doi.org/10.1016/j.fuel.2024.131897
Received 18 September 2023; Received in revised form 16 April 2024; Accepted 12 May 2024
Available online 24 May 2024

Table 1
Boundary conditions used in the experiments [19].

#	Equivalence ratio φ	V_{in} (cm/s)	Plate temperature T_W (K)
1	0.57	23.4	489.7
2	0.585	24.26	491.3
3	0.6	25.53	493.5
4	0.65	27.09	496.6
5	0.7	27.93	499.2
6	0.75	29.18	503.8
7	0.8	31.26	511.5
8	1.0	42.57	563.6
9	1.2	40.96	574.7
10	1.4	30.86	504.0

and the pollutants that can be released by the combustion of these fossil fuels include CO_2, CO, NOx, SO_2, volatile compounds, particulate matter, etc. which have extremely negative impacts on the ecosystem [1]. Due to the negative effects of CO_2, it has been necessary to develop new technologies that aim to reduce problems that correlate with energy consumption. These factors combined with more strict regulations lead to investigate carbon-free fuel sources linked to renewable energy resources [2]. Ammonia (NH_3) is a promising alternative carbonless fuel due its high hydrogen density content, hence making it an attractive hydrogen carrier fuel. The fuel enables 1) CO_2, SOx and soot emission free flue gases; 2) producibility from different sources such as renewable sources and biomass; 3) transportation and storage can be done using working existing infrastructure. All these factors make NH_3 a favourably clean fuel candidate for the energy sector. However, high NOx emission and narrow flammability limits are the main problem that restricts the use of NH_3 in large-scale thermal devices [3,4]. The combustion properties of NH_3, in terms of laminar burning velocity, have been studied and improved by blending NH_3 with other doping agents as a fuel. However, this can increase NOx emissions [3–6].

The term NOx stands for all nitrogen oxide forms generated by combustion, which are mainly nitric oxide (NO), nitrogen dioxide (NO_2) and nitrous oxide (N_2O). The greenhouse effect of N_2O is also very important as it has 300 times larger Global Warming Potential than CO_2 [7,8]. Several experimental and numerical studies have been carried out on NH_3-H_2 blends in terms of N_2O emission [9–11]. A study on turbulent swirl-stabilized ammonia/hydrogen flames using a tangential swirl burner by Alnasif et al. [9] identified that the concentration of N_2O peaks at an 85/15 vol% NH_3/H_2 blend with a thermal power of 20 kW and a Reynolds number of 40,000. Another study conducted by Okafor et al. [12] on turbulent, swirl-stabilized ammonia/air flames indicated that heat loss promotes N_2O emissions. However, due to the complex flow structure within a swirl combustor, it is challenging to analyse the production and reduction mechanisms of N_2O, making this study unavailable for chemistry validation. Numerically, many studies have been carried out on NH_3 in terms of understanding the chemical kinetics of NH_3 combustion to improve the reaction mechanism of NOx. The performance of most advanced kinetic models was improved on the basis of experiments conducted on many combustion configurations, an exercise that resulted in adding new reactions or updating rate parameters that govern the rate of reactions [13–16].

Table 2
Kinetic reaction mechanisms adopted in the present study.

#	Kinetic mechanism	No. of reactions	No. of species	Ref.	#	Kinetic mechanism	No. of reactions	No. of species	Ref.
1	Bertolino et al., 2021	264	38	[23]	35	Dagaut et al., 2008	250	41	[24]
2	Mei et al., 2021	264	38	[25]	36	Gregory P. Smith et al., 2000	325	53	[26]
3	Han et al., 2021	298	36	[27]	37	Coda Zabetta and Hupa, 2008	371	60	[28]
4	Tang, et al., 2022	211	35	[29]	38	Alzueta MU, 2016	654	131	[30]
5	Gotama et al., 2022	119	26	[13]	39	Shmakov et al., 2010	1207	127	[31]
6	Shrestha et al., 2021	1099	125	[32]	40	Esarte et al., 2011	536	79	[33]
7	Z. Wang et al., 2021	444	91	[34]	41	Abian et al., 2015	201	31	[35]
8	X. Zhang et al., 2021	263	38	[18]	42	T. Wang et al., 2018	925	81	[36]
9	Arunthanayothin et al., 2021	2444	157	[37]	43	T. Faravelli, 2017	158	29	[38]
10	Stagni et al., 2020	203	31	[16]	44	POLIMI, 2014	155	29	[39]
11	Han et al., 2019	177	35	[40]	45	Marques et al., 2009	318	61	[41]
12	De Persis et al., 2020	647	103	[42]	46	Aranda et al., 2013	566	95	[43]
13	Mei et al., 2019	265	38	[44]	47	Jiang et al., 2020	60	19	[45]
14	Li et al., 2019	957	128	[46]	48	Sun et al., 2022	486	66	[47]
15	Okafor et al., 2019	356	59	[48]	49	Song et al., 2019	158	29	[49]
16	Glarborg et al., 2018	231	39	[50]	50	Mével et al., 2009	203	32	[51]
17	Shrestha et al., 2018	1081	124	[52]	51	Da Rocha et al., 2019 (Improved Mathiue mech.)	66	22	[53]
18	Otomo et al., 2018	213	32	[54]	52	Da Rocha et al., 2019 (Improved Otomo mech.)	51	21	[53]
19	U. Mechanism, 2018	41	20	[55]	53	Da Rocha et al., 2019 (Improved Okafor mech.)	70	24	[53]
20	Klippenstein et al., 2018	211	33	[56]	54	Kovaleva et al., 2022	354	59	[57]
21	Nakamura et al., 2017	232	33	[14]	55	Houshfar et al., 2012 (Midd temp.)	91	26	[58]
22	Y. Zhang et al., 2017	251	44	[59]	56	Houshfar et al., 2012 (High temp.)	430	52	[58]
23	Lamoureux et al., 2016	934	123	[60]	57	Houshfar et al., 2012 (Low temp.)	198	35	[58]
24	Xiao et al., 2017	276	55	[61]	58	Capriolo et al., 2021	2300	201	[62]
25	Song et al., 2016	204	32	[63]	59	Xu et al., 2023	389	69	[64]
26	Nozari and Karabeyoğlu, 2015	91	21	[65]	60	Thomas et al., 2022	1099	125	[66]
27	Mathieu and Petersen, 2015	278	54	[67]	61	Kovács et al., 2020	214	34	[68]
28	Duynslaegher et al., 2012	80	19	[69]	62	Kovács et al., 2021	537	70	[70]
29	Klippenstein et al., 2011	202	31	[71]	63	Saxena and Williams, 2007	288	59	[72]
30	K. Zhang et al., 2011	701	88	[73]	64	Valkó et al., 2022	537	70	[74]
31	Lamoureux et al., 2010	883	119	[75]	65	Alzueta et al., 2001	464	65	[76]
32	Konnov, 2009	1207	127	[77]	66	Nakamura and Shindo, 2019	485	66	[78]
33	Mendiara and Glarborg, 2009	779	79	[79]	67	Glarborg, 2022	270	41	[15]
34	Tian et al., 2009	703	84	[80]					

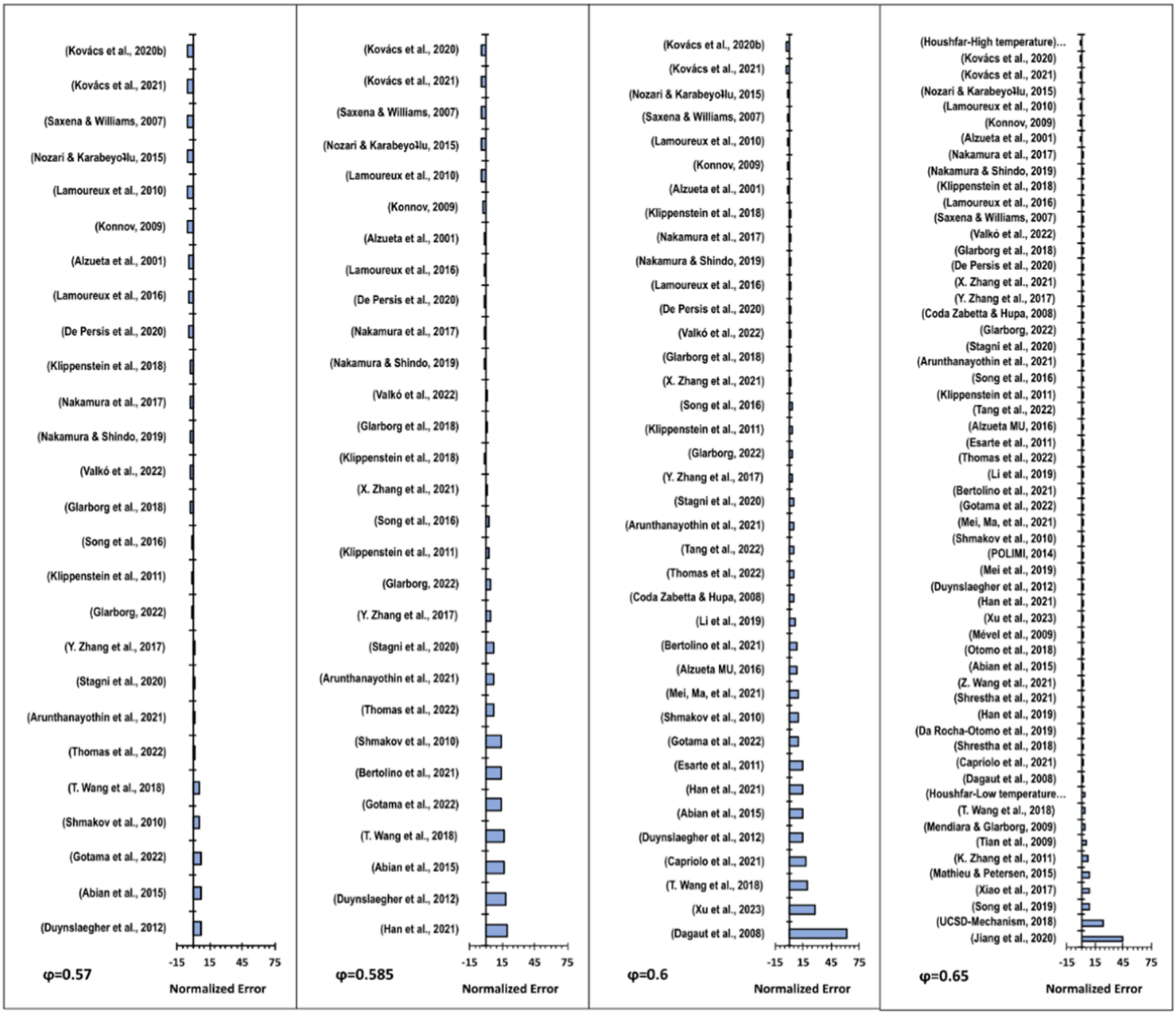

Fig. 1. Normalized error of N_2O mole fractions for 67 reaction mechanisms in lean NH_3/H_2 flames, analysed using BSSF numerical data across equivalence ratios of 0.57 to 0.65. Notably, at conditions of 0.57, 0.585, and 0.6, numerous tested kinetic models failed to predict the N_2O mole fractions.

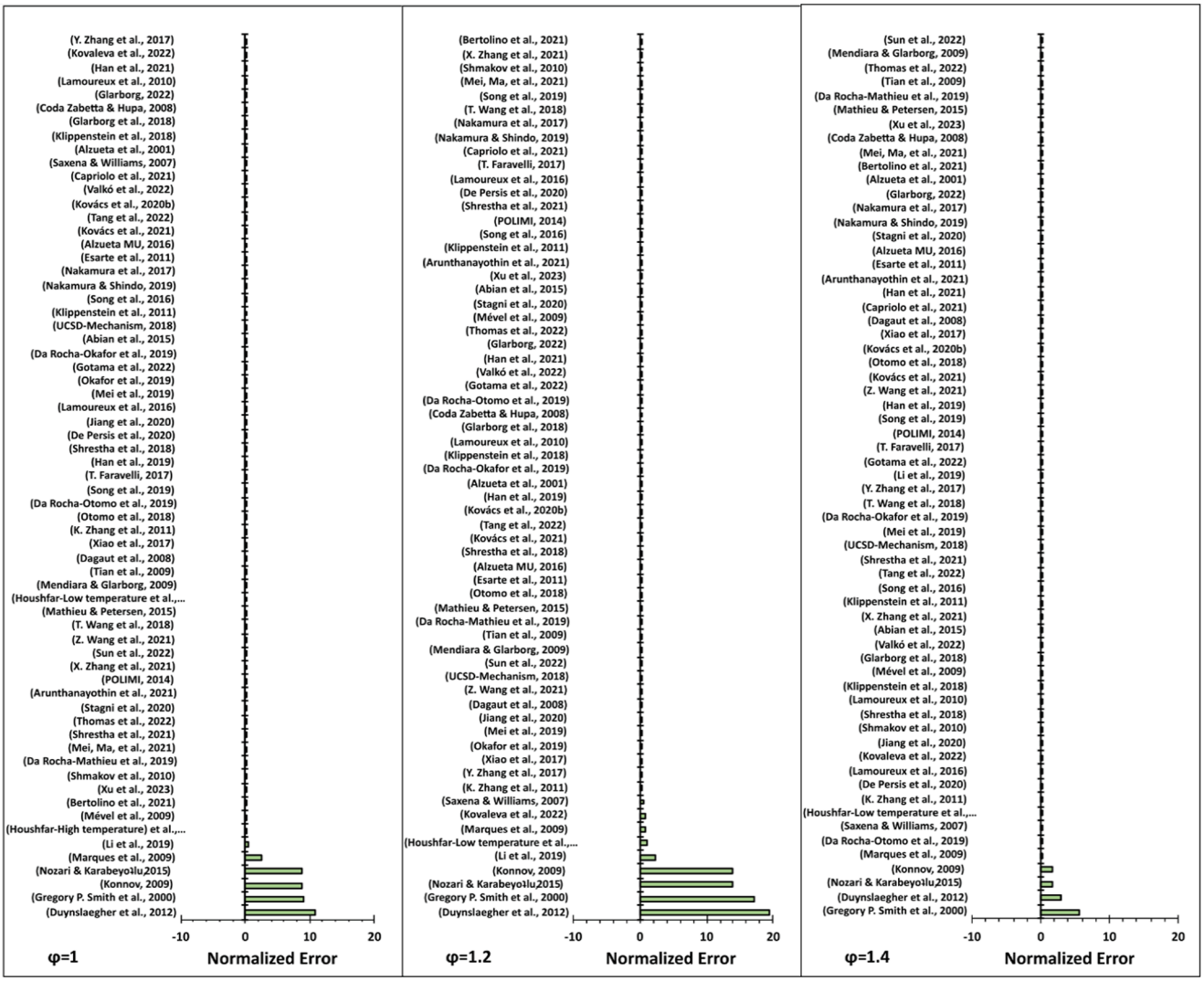

Fig. 2. Normalized Error of N_2O Mole Fractions for 67 Reaction Mechanisms in stoichiometry and rich NH_3/H_2 Flames, Analysed Using BSSF Numerical Data Across Equivalence Ratios of 1 to 1.4.

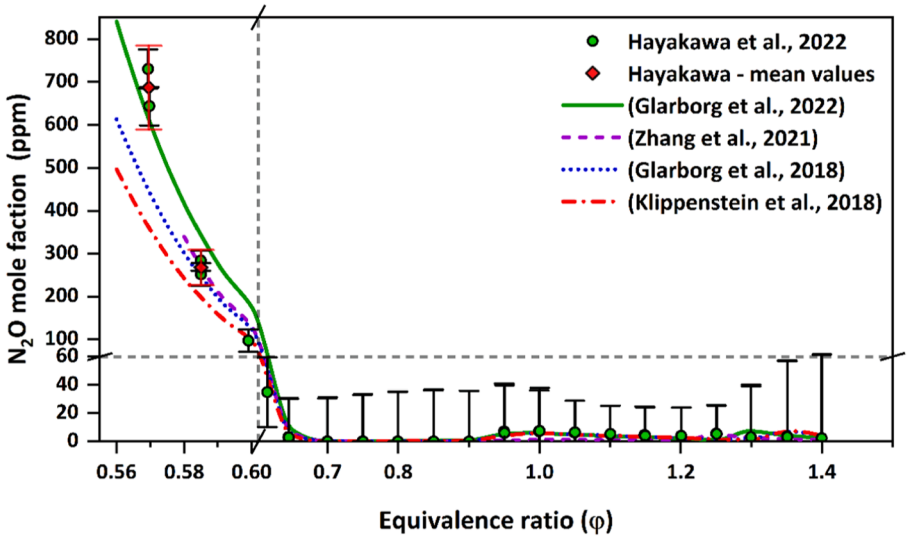

Fig. 3. Variation of N_2O mole fraction as a function of equivalence ratio for 70/30 vol% NH_3/H_2 premixed flames using the Burner Stabilized Stagnation Flame Model (BSSF). The symbols denote experimental data, while the dotted lines represent simulation results. Scale breaks, shown as dashed grey lines, were introduced to show data variations across all scales clearly.

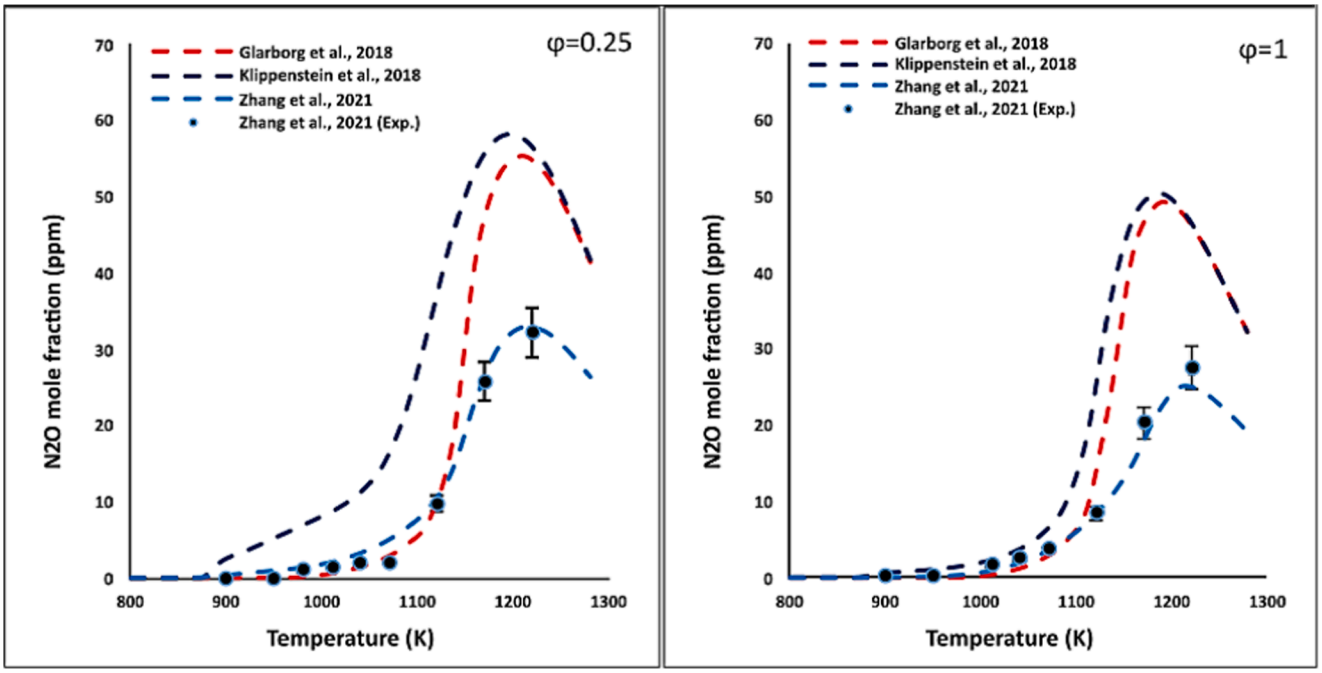

Fig. 4. Variation of N_2O mole fractions with temperature at equivalence ratios of 0.25 and 1. Experimental results are depicted by symbols, while simulations are illustrated with dotted lines. The model from Zhang et al. [18] has been fitted based on data reported in their study, explaining the close match observed above.

According to studies by Valera Medina et al. [3] and Mørch et al. [17], a 70/30 vol% NH_3/H_2 blended fuel provides stable performance in fuelling gas turbine combustors. This blend has been selected for consideration in the present study. The literature on the experimental investigation of ammonia combustion has been extensively reviewed. To the best of our knowledge, the data chosen for validation, published by Zhang et al. [18] and Hayakawa et al. [19], is the only dataset found in the literature for N_2O speciation of a 70/30 vol% NH_3/H_2 blend at atmospheric conditions and various equivalence ratios. In the study by Zhang et al. [18], NH_3/H_2 mixtures were investigated using jet-stirred reactor (JSR) oxidation experiments at atmospheric pressure, covering a temperature range of 800–1280 K and two equivalence ratios (0.25 and 1). The data collected from these experiments helped refine their kinetic model, improving its ability to accurately predict the mole fractions of NO and N_2O under the conditions tested. Hayakawa and coworkers used the same system configuration (stabilized-stagnation flame configuration) as Brackmann et al. [20]. This configuration allows the flame to be stabilized without a pilot flame or the addition of chemical species to enhance flame intensity, which is a beneficial strategy for ammonia flames in terms of: 1) Temperature Distribution: The stagnation point heats up due to gas compression, aiding complete ammonia combustion. 2)Uniformity: Symmetrical gas flow creates even temperature and gas concentration, ensuring consistent product gases. 3)Stability: The steady gas flow at the stagnation point maintains a stable flame, which is less vulnerable to disturbances, ensuring consistent production of combustion products. These factors can influence combustion efficiency and NOx formation accuracy, reducing the amount of unburned fuel in the product gases. Furthermore, a stagnation-stabilized flame configuration can be easily simulated using CHEMKIN software [21] by applying the appropriate boundary conditions.

Given the aforementioned, selecting the dataset provided by Hayakawa et al. [19] for validation is advantageous. The only issue is the large uncertainty bars, which can be attributed to the FTIR gas analyser used for collecting gas products. This analyser is designed to measure up to 1000 ppmv, and when measuring N_2O at this upper limit, the results are less precise, with a significant margin of error or uncertainty, as mentioned by the group in another published work on ammonia flames [22]. The current study aims to analyse the performance of kinetic reaction mechanisms for estimating N_2O in a 70/30 vol% NH_3/H_2 blended fuel at the full range of equivalence ratios (0.57–1.4). Additionally, the study aims to identify the reaction steps responsible for N_2O formation/consumption and reveal the reasons for discrepancies in the estimation of experimental measurements of N_2O in ammonia combustion systems.

2. Numerical setup and kinetic modeling

Chemkin-Pro package of ANSYS software was used to study the performance of 67 chemical kinetic mechanisms in stabilised-stagnation flame simulations (BSSF). The numerical simulations applied the same boundary conditions as those used in the experiments in terms of atmospheric conditions, plate temperature and inlet velocity of the blend, Table 1. Also, the length of the computational domain was set to 2 cm in accordance with the distance of the top plate from the nozzle burner used in the experiments. In addition, the Soret effect (Thermal diffusion effect) was considered in this study due to the exothermic nature of combustion reactions. Further, the maximum number of grid points allowed with adaptive grid control, gradient and curvature thresholds were set to 5000, 0.01, 0.01, respectively.

Table 2 lists the tested kinetic reaction mechanisms in this present study in terms of the number of species and reactions. The experimental measurements for data validation were selected from the published work of [19]. The authors employed a stagnation flame configuration system to determine the mole fraction of N_2O from the combustion of a 70/30 (vol%) NH_3/H_2 blended fuel. This approach was chosen to avoid stabilization issues, which leads to more consistent production of combustion products and enables the obtaining of accurate measurements.

To examine the effect of equivalence ratio on the N_2O mole fractions, various equivalence ratios have been applied in the range of 0.57–1.4. A top stagnation plate was fixed 2 cm above the outlet section of the burner to manage generating a stagnation flow. The values of the top plate surface temperature (T_W) and the mixture inlet velocity (V_{in}) were varied because of the variation in equivalence ratios and this variation changed the laminar burning velocity. The experimental data from [19] have been selected as it matched the conditions of our interest in terms of NH_3/H_2 ratio, the range of the equivalence ratio and the standard

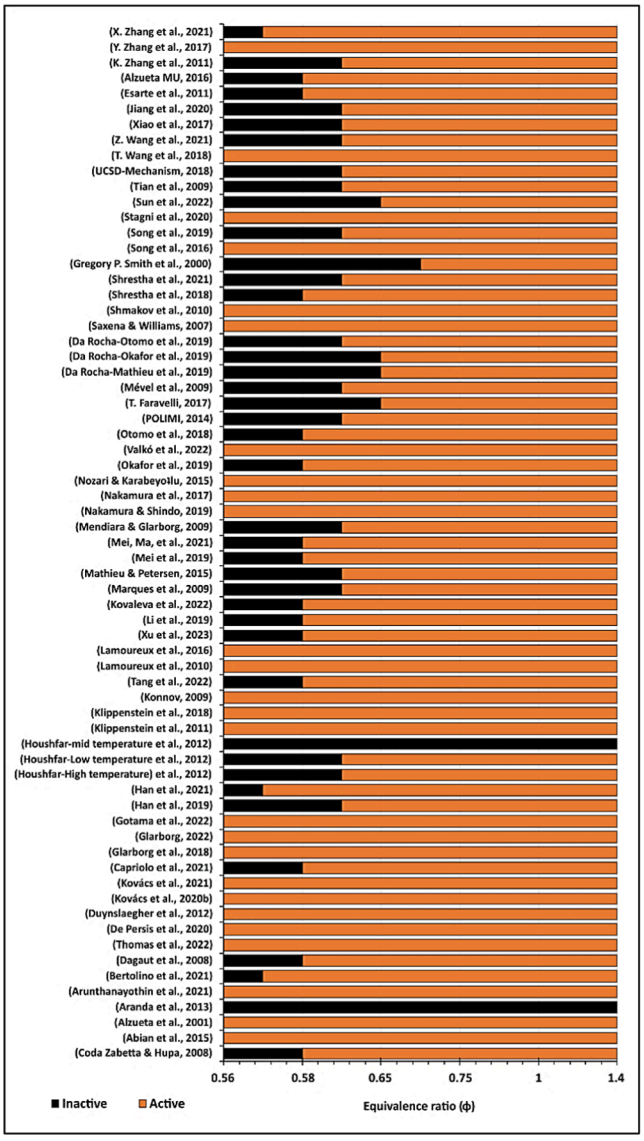

Fig. 5. Comparative analysis of kinetic reaction mechanisms in terms of evaluating activation performance for ignition versus inactivity resulting in ignition failure.

conditions of the unburned gas. In the current study, a normalized error method was chosen as an initial metric for adjusting the discrepancy between a numerical result and an experimental finding [19], considering the uncertainty in the measurements, as illustrated in Eq.1. The N_2O mole fractions obtained from experimental data tend to be near zero, especially in the φ range of 0.65–1.4, which results in considerable uncertainties. Therefore, adjusting for uncertainty is important as it provides context for the discrepancy. A minor difference between the experimental and theoretical values could be meaningful if the uncertainty is very low, while a more substantial difference might be less relevant if the uncertainty is high.

$$Normalised\ Error = \frac{F_t - A_t}{Uncertainity} \quad (1)$$

Where F_t: is the forecast from numerical calculations; and A_t: is the actual value from experiments.

3. Results and discussion

Fig. 1 and Fig. 2 illustrate the performance of the mechanisms by comparing their simulation results with experimental measurements, taking into account the uncertainty in these measurements within the ranges of φ (0.57–0.65) and (1–1.4), respectively. This approach helps identify reaction mechanisms that demonstrate a low discrepancy with the experimental results. Meanwhile, Fig. 3 displays the variation in the mole fraction of N_2O as a function of the equivalence ratio over the range of 0.56 to 1.4. The mole fraction of N_2O was measured at the end of the computational domain (at X = 2 cm), corresponding to the sampling point for the experimental emissions under steady-state conditions. As shown in Fig. 3, and in line with the experimental measurements reported by the Hayakawa et al. [19], the N_2O concentration drops exponentially in the range of φ = 0.56–0.7, to very low undefined values (the authors consistently reported negative concentration values, with a mean of −1.92 ppm and a standard deviation of 0.43 ppm, in the φ = 0.7–0.9 range). Subsequently, the concentration increases, reaching a peak of over 7.5 ppm at the stoichiometric condition, and then decreases to 2 ppm as it is approaching the rich φ = 1.4 condition. These systematic changes at low concentrations are captured by the selected mechanisms, as depicted in Fig. 3. The one standard deviation of statistical noise for the N_2O data in the φ = 1.0–1.4 region, estimated using the Minimal Spline Fit code [81], was found to be 0.4 ppm. This value is 50–150 times lower than the error bars proposed by the authors, suggesting that the evaluated uncertainty in this range is primarily composed of systematic errors and might be overly conservative.

Regarding the uncertainty of equivalence ratios, in the study by Hayakawa [19], the authors carefully analysed the N_2O concentration uncertainties. However, they did not discuss the uncertainty of equivalence ratios and their impact. Instead, they noted in their paper that the accuracy of the mass flow meter for NH_3 and H_2 is ± 1.0 % FS, and for air, it is ± 1.5 % FS. Considering the information provided, the Gaussian error propagation results in a 1.8 % uncertainty in equivalence ratios, corresponding to a 0.01 uncertainty at the leanest conditions. They also applied parallel measurements at rounded equivalence ratios to assess the reproducibility of the measurements used in their investigations. The scatter of data from parallel measurements is particularly noticeable at lean equivalence ratios (0.57 and 0.585), which should be attributed to the significant value of equivalence ratio uncertainty (approximately 0.01). For assessing mechanism performance under these conditions, the average of the measured values was taken, with an increased error bar derived from the deviation between the two values ($\Delta = x_1 - x_2$), and their uncertainties (error bars correspond to $\pm 2\sigma_{1,2}$). The uncertainties are calculated as follows: $\sigma^2_{mean} = (\Delta/2)^2 + (\sigma_1^2 + \sigma_2^2)/2$.

Additional validation using jet-stirred reactor measurements has been adopted to assess the accuracy and generalisability of the well-performing kinetic models in the burner-stabilised stagnation configuration. This approach, based on the study by Zhang et al. [18], involves 70/30 vol% NH_3/H_2 mixtures at atmospheric pressure, covering temperatures from 800 to 1280 K and two equivalence ratios, φ (0.25 and 1). The simulation process utilised a transient, perfectly stirred reactor model. Simulation parameters such as end times, boundary conditions, and mesh conditions were carefully applied, following the methodologies detailed in the study by Zhang et al. [18].

As illustrated in Fig. 4, the Glarborg kinetic model exhibits excellent performance in the temperature range of 900 K to 1120 K when φ is set to 0.25. However, its performance declines above 1150 K, marked by an overprediction of the N_2O mole fraction. In contrast, the Klippenstein model consistently overpredicts across the tested temperature range. When the equivalence ratio is increased to 1, the Glarborg model maintains its performance, showing a similar prediction trend as at a φ of 0.25. Meanwhile, the Klippenstein model shows improved performance, accurately predicting within the range of 900 K to 1040 K but overestimating N_2O mole fractions above 1040 K. The kinetic model of Zhang et al. [18], refined based on the provided experimental measurements, as shown in Fig. 4, was also used to validate the experimental

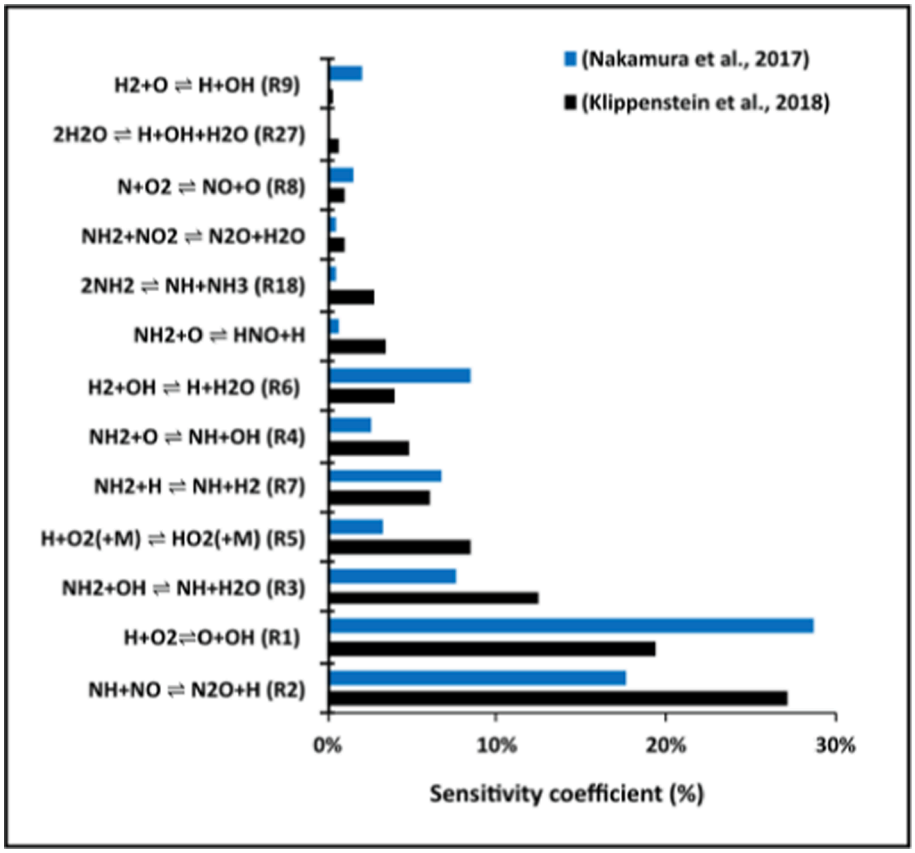

Fig. 6. Reactions with the largest positive sensitivity coefficients for N_2O mole fractions in 70/30 vol% NH_3/H_2 premixed flame at $\varphi = 0.6$ in the Klippenstein and Nakamura kinetic models.

measurements of Hayakawa et al. [19], as depicted in Fig. 3. This comparison was conducted to assess its predictive accuracy against other selected models and combustion configurations. The Zhang mechanism provides an excellent estimation of N_2O mole fractions, closely matching the trend estimated by the Glarborg model, except for a tendency to overpredict N_2O mole fractions when φ exceeds 0.6. Under these conditions, the Klippenstein model falls within the range of uncertainty measurements, offering a better estimation.

Given the varying trends of N_2O mole fractions in the burner-stabilized stagnation flame model at different equivalence ratios, the analysis has been divided into three categories: lean ($\varphi = 0.6$), stoichiometric ($\varphi = 1$), and rich flames ($\varphi = 1.4$). This categorization is based on the modelling of 70/30 vol% NH_3/H_2 blend within this specific flame model. A sensitivity analysis, along with an investigation of the rate of N_2O production/consumption, will be conducted for each category. The aim is to clarify the differences among the selected mechanisms and to identify the key reactions contributing to N_2O formation.

Fig. 1 clearly shows that most of the tested kinetic reaction mechanisms are not included, particularly in the range of 0.57 to 0.6, due to performance issues. The simulations of these models yield zero mole fractions of N_2O, in contrast to the experimental measurements, which indicate a high value of N_2O concentration, as seen in Fig. 3. Further investigation revealed that most of the tested mechanisms failed to meet the combustion requirements under the specified conditions; this was indicated by the ammonia concentration remaining constant, showing no consumption. This occurred despite the solution being grid-independent, as illustrated in Fig. 5.

Consequently, these mechanisms have been excluded from the investigation under their determined conditions, as shown in Fig. 5. The failure to achieve ignition, as observed, might be attributed to kinetic inhibition, a scenario where the reaction rates of key steps in the mechanism are too slow to initiate or sustain combustion. Additionally, the mechanisms proposed by Houshfar et al. [58] for NOx chemistry in the medium-temperature range, along with those by Aranda et al. [43] have been excluded from further investigations. This exclusion is based on two primary considerations: the absence of a comprehensive sub-mechanism for NH_3 in Aranda's kinetic model and the lack of N_2O chemistry in Houshfar.'s chemistry database.

3.1. *Lean flame conditions*

Fig. 3 illustrates the variation in the mole fraction of N_2O as a function of the equivalence ratio (φ) within the range of 0.56 to 1.4. It demonstrates that the N_2O mole fraction decreases sharply, approaching nearly zero, as φ increases. According to the normalized error trends in lean flame conditions (0.585–0.65), as shown in Fig. 1, the reaction mechanisms of Glarborg [50] and Klippenstein [56] provide a good estimation of N_2O mole fraction when their outcomes are compared with the experimental measurements, considering the measurement uncertainty along the lean range of 70/30 vol% NH_3/H_2 blended fuel. However, their performance deteriorates at an equivalence ratio of 0.57, where the Klippenstein mechanism underestimates the mole fraction of N_2O with a normalized error by 3.4, and the Glarborg mechanism by 2.5. Their performance improves, however, as the equivalence ratio increases, where their normalized error values are less than one. According to Fig. 1, the Nakamura kinetic model [14] shows a high level of accuracy in estimating the error for N_2O mole fractions at $\varphi = 0.6$, while Klippenstein's mechanism demonstrates better performance than Glarborg's model. Since all the aforementioned mechanisms have minor differences in normalized error, it is worthwhile to investigate the reasons behind this. Therefore, both kinetic models, i.e., Nakamura and Klippenstein, will be investigated in detail with local sensitivity and rate

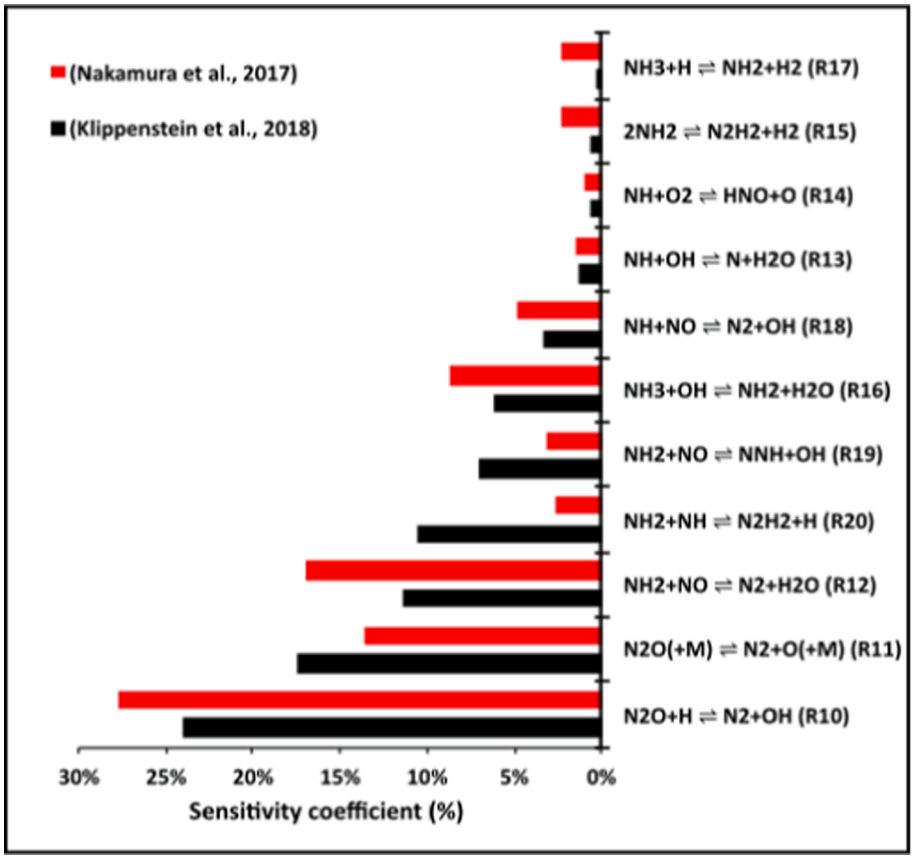

Fig. 7. Reactions with the largest positive sensitivity coefficients for N_2O mole fractions in 70/30 vol% NH_3/H_2 premixed flame at $\varphi = 0.6$ predicted by the Klippenstein and Glarborg kinetic models.

of production/consumption analysis of N_2O to reveal the reasons behind the discrepancies among the selected mechanisms.

Fig. 6 and Fig. 7 show the reactions with the largest positive and negative sensitivity coefficients for N_2O mole fraction in the Nakamura and Klippenstein mechanisms. These coefficients are normalized to their respective sums and presented as percentages. As observed in Fig. 6, reactions $H + O_2 \rightleftharpoons O + OH$ (**R1**) and $NH + NO \rightleftharpoons N_2O + H$ (**R2**) play a major role in increasing N_2O mole fractions; they also enhance the system reactivity by generating reactive H, O, and OH radicals. Additionally, the promoting effect of the reactions $NH_2 + OH \rightleftharpoons NH + H_2O$ (**R3**), $NH_2 + O \rightleftharpoons NH + OH$ (**R4**), $H + O_2(+M) \rightleftharpoons HO_2(+M)$ (**R5**), $H_2 + OH \rightleftharpoons H + H_2O$ (**R6**), and $NH_2 + H \rightleftharpoons NH + H_2$ (**R7**) is clear in both selected mechanisms, contributing to an increase in N_2O mole fraction through the production of more NH and OH radicals. These NH radicals are highly reactive and tend to react with NO to produce N_2O via the reaction $NH + NO \rightleftharpoons N_2O + H$ (R2). Moreover, both selected kinetic models show varying trends in sensitivity coefficients. The reaction steps R1, R6, $N + O_2 \rightleftharpoons NO + O$ (**R8**), and $H_2 + O \rightleftharpoons H + OH$ (**R9**) exhibit higher levels of positive sensitivity coefficients towards promoting the formation of N_2O mole fractions in Nakamura's model compared to the Klippenstein mechanism. This discrepancy is attributed to the mechanistic differences between the tested models, specifically in terms of the rate parameters of the aforementioned reactions, which dictate the reaction rates of each key reaction (see to Table 3).

As shown in Fig. 7, both selected kinetic models identify the same key reactions involved in mitigating N_2O formation. The reaction steps $N_2O + H \rightleftharpoons N_2 + OH$ (**R10**), $N_2O(+M) \rightleftharpoons N_2 + O(+M)$ (**R11**), and $NH_2 + NO \rightleftharpoons N_2 + H_2O$ (**R12**) play a significant role in reducing the mole fraction of N_2O, as they exhibit large negative sensitivity coefficients that impact N_2O production. A negative sensitivity coefficient for a reaction implies that an increase in the reaction rate leads to a decrease in the concentration of the species involved. Therefore, the negative coefficients for reactions R10, R11, and R12 in both selected mechanisms suggest that an increased rate of these reactions results in a lowered concentration of N_2O. Notably, the reaction steps $NH + OH \rightleftharpoons N + H_2O$ (**R13**) and $NH + O_2 \rightleftharpoons HNO + O$ (**R14**) show roughly the same sensitivity coefficient values in both models. Furthermore, the reaction steps R10, R12, $2NH_2 \rightleftharpoons N_2H_2 + H_2$ (**R15**), $NH_3 + OH \rightleftharpoons NH_2 + H_2O$ (**R16**), $NH_3 + H \rightleftharpoons NH_2 + H_2$ (**R17**), and $NH + NO \rightleftharpoons N_2 + OH$ (**R18**) show higher negative sensitivity coefficient values in Nakamura's model compared to those predicted by Klippenstein's kinetic model. Conversely, Klippenstein's model demonstrates slightly higher levels of sensitivity coefficients towards the reaction steps R11, $NH_2 + NO \rightleftharpoons NNH + OH$ (**R19**), and $NH_2 + NH \rightleftharpoons N_2H_2 + H$ (**R20**) than Nakamura's model. The variation in sensitivity coefficients is attributed to the differences in rate parameters between the models, which govern the rate coefficient of each reaction step, as detailed in Table 3.

To explain the reasons behind the discrepancies in the performance of the Klippenstein mechanism [56] compared to the Glarborg kinetic model [50], a sensitivity analysis was conducted under the same conditions ($\varphi = 0.6$) for both models. This analysis aimed to identify which reactions or parameters critically influence the behaviour of the system in each model. Fig. 8 and Fig. 9 showcase the reactions with the largest positive and negative sensitivity coefficients for N_2O mole fraction in the Glarborg and Klippenstein mechanisms, respectively. These Figures clearly illustrate the differences in mechanistic behaviour, particularly in terms of the rate parameters that control the key reactions. Both selected mechanisms highlight the crucial role of reaction steps R1, R2, R3, and R5 in promoting the formation of N_2O. Notably, both models exhibit nearly identical trends for sensitivity coefficients, with the exception of the key reactions R1 and R5, which is predicted by Glarborg's model to have a higher sensitivity coefficient value for

Table 3
Key reactions of N_2O formation generated from Klippenstein, Nakamura, Zhang, and Sun kinetic models.

NO.	Reaction	(Klippenstein et al., 2018)			(Nakamura et al., 2017)			(Y. Zhang et al, 2017)			(Sun et al, 2022)		
		A	***n***	***E***	***A***	***n***	***E***	***A***	***n***	***E***	***A***	***n***	***E***
(R1)	$H + O_2 \rightleftharpoons O + OH$	1.00E+14	0.00	15,286	1.040E+14	0.00	15,286	1.000E+14	0.00	15,286	1.00E+14	0.00	15,286
(R2)	$NH + NO \rightleftharpoons N_2O + H$	2.7E+15	−0.780	20	1.800E+14	−0.351	−244	1.80E+14	0.351	−244	3.65E+14	−0.45	0.00
(R3)	$NH_2 + OH \rightleftharpoons NH + H_2O$	3.3E+06	1.949	−217	4.0E+06	2.00	1000	3.3E+06	1.949	−217	3.3E+06	1.949	−217
(R4)	$NH_2 + O \rightleftharpoons NH + OH$	8.6E-1	4.010	1673	6.750E+12	0	0	–	–	–	–	–	–
(R5)	$H + O_2(+M) \rightleftharpoons HO_2(+M)$	4.7E+12	0.440	0	4.650E+12	0.44	0	4.650E+12	0.440	0	2.8E18	−0.86	0.00
(R6)	$H_2 + OH \rightleftharpoons H + H_2O$	2.2E+08	1.51	3430	4.380E+13	0.00	6990	4.380E+13	0.00	6990	2.16E+08	1.51	3430
(R7)	$NH_2 + H \rightleftharpoons NH + H_2$	2.1E+13	0.000	15,417	6.920E+13	0.00	3650	7.2E+05	2.32	799	1.000E+6	2.32	7990
(R8)	$N + O_2 \rightleftharpoons NO + O$	6.4E+09	1.000	6280	6.4E+09	1.00	6280	9.03E+09	1.00	6498	9.0E+09	1.00	6500
(R9)	$H_2 + O \rightleftharpoons H + OH$	3.8E+12	0.000	7948	–	–	–	5.080E+04	2.67	6292	3.87E+4	2.7	6260
(R10)	$N_2O + H \rightleftharpoons N_2 + OH$	6.4E+07	1.835	13,492	3.310E+10	0.00	5090	6.4E+07	1.835	13,492	3.31E+10	0.00	5090
(R11)	$N_2O(+M) \rightleftharpoons N_2 + O(+M)$	6.0E+14	0.000	57,444	6.620E+14	0.00	57,500	7.2E+14	0.000	57,410	6.62E+14	0.00	57,500
(R12)	$NH_2 + NO \rightleftharpoons N_2 + H2O$	2.6E+19	−2.369	870	–	–	–	1.36E+16	−1.25	0.0	3.10E+13	−0.48	1180
(R13)	$NH + OH \rightleftharpoons N + H_2O$	1.6E+07	1.733	−576	5.0E+11	0.50	2000	1.6E+07	1.733	−576	–	–	–
(R14)	$NH + O_2 \rightleftharpoons HNO + O$	2.4E+13	0.00	13,850	1.0E+13	0.00	12,000	1.75E+12	0.114	11,055	–	–	–
(R15)	$2NH_2 \rightleftharpoons N_2H_2 + H_2$	1.7E+08	1.62	11,783	5.0E+13	0.00	10,000	–	–	–	–	–	–
(R16)	$NH_3 + OH \rightleftharpoons NH_2 + H_2O$	2.0E+06	2.040	566	3.250E+12	0.00	2120	2.0E+06	2.040	566	2.0E+06	2.040	566
(R17)	$NH_3 + H \rightleftharpoons NH_2 + H_2$	6.4E+05	2.390	10,171	6.40E+05	2.390	10,171	–	–	–	6.4E+05	2.390	10,171
(R18)	$NH + NO \rightleftharpoons N_2 + OH$	6.8E+14	−0.780	20	–	–	–	2.70E+12	−0.072	−512	2.70E+12	−0.072	−512
(R19)	$NH_2 + NO \rightleftharpoons NNH + OH$	4.3E+10	0.294	−866	3.100E+13	−0.48	1180	3.100E+13	−0.48	1180	4.3E10	0.294	−870
(R20)	$NH_2 + NH \rightleftharpoons N_2H_2 + H$	4.3E+14	−0.272	−77	1.500E+15	−0.50	0.00	4.30E+14	−0.272	−77	1.50E+15	−0.5	0.00
(R21)	$2NH_2 \rightleftharpoons NH + NH_3$	5.6E+00	3.530	552	–	–	–	–	–	–	5.6000E0	3.53	552
(R22)	$NH_2 + O \rightleftharpoons HNO + H$	6.6E+13	0.00	0.00	4.60E+13	0.00	0.00	6.600E+13	0.00	0.0	3.90E+13	0.00	0.0
(R23)	$NH_2 + NO_2 \rightleftharpoons N_2O + H_2O$	2.2E+11	0.110	−1186	1.60E+16 –	1.44	268	3.0E+14	0.77	242	2.60E+18	−2.191	455
(R24)	$2H_2O \rightleftharpoons H + OH + H_2O$	1.0E+26	−2.440	120,180	–	–	–	–	–	–	–	–	–
(R25)	$N_2O + O \rightleftharpoons 2NO$	9.2E+13	0.000	27,679	9.150E+13	0.00	27,693	–	–	–	–	–	–
(R26)	$N_2O + O \rightleftharpoons N_2 + O_2$	9.2E+13	0.000	27,679	3.690E+12	0.00	15,944	–	–	–	–	–	–
(R27)	$N_2H_2 + NO \rightleftharpoons N_2O + NH_2$	4.0E+12	0.000	11,922	3.000E+10	0.00	0.00	4.0E+12	0.0	11,922	4.00E+12	0.00	11,922
(R28)	$NH + OH \rightleftharpoons HNO + H$	3.2E+14	−0.376	−46	–	–	–	3.20E+14	−0.376	−46	3.20E+14	−0.376	−46.0
(R29)	$N + NO \rightleftharpoons N_2 + O$	9.4E+12	0.140	0	1.00E+14	0.00	75,490	11.28E+12	0.14	0.0	9.40E+12	0.14	0.00
(R30)	$N_2O + H_2 \rightleftharpoons N_2 + H_2O$	–	–	–	–	–	–	2.100E+14	0.0	32,500	9.4E+12	0.140	0
(R31)	$NH + NO_2 \rightleftharpoons N_2O + OH$	4.1E+12	0.00	0.00	1.00E+13	0.00	0.00	4.1E+12	0.000	0.000	4.1E12	0.000	0.000
(R32)	$2HNO \rightleftharpoons N_2O + H_2O$	9.0E+08	0.00	3100	3.950E+12	0.00	5000	9.0E+08	0.00	3100	3.950E12	0.00	5000
(R33)	$HNO + NO \rightleftharpoons N_2O + OH$	1.20E-4	4.330	25,080	2.000E+12	0.00	26,000	1.20E-4	4.330	25,080	2.00E+12	0.00	2600
(R34)	$NNH + O \rightleftharpoons N_2O + H$	1.9E+14	−0.274	–22	–	–	–	1.9E+14	−0.274	–22	1.90E+14	−0.274	–22.0
(R35)	$N + OH \rightleftharpoons NO + H$	3.8E+13	0.00	0.00	–	–	–	–	–	–	–	–	–
(R36)	$H + O_2 + H_2O \rightleftharpoons HO_2 + H_2O$	–	–	–	–	–	–	–	–	–	1.126E+19	−0.76	0.00
(R37)	$N_2H_3 \rightleftharpoons N_2H_2 + H$	1.3E+14	0.00	3871	–	–	–	–	–	–	3.6E+47	−10.38	69,009

*Units are cm^3, mol, s, cal, K.

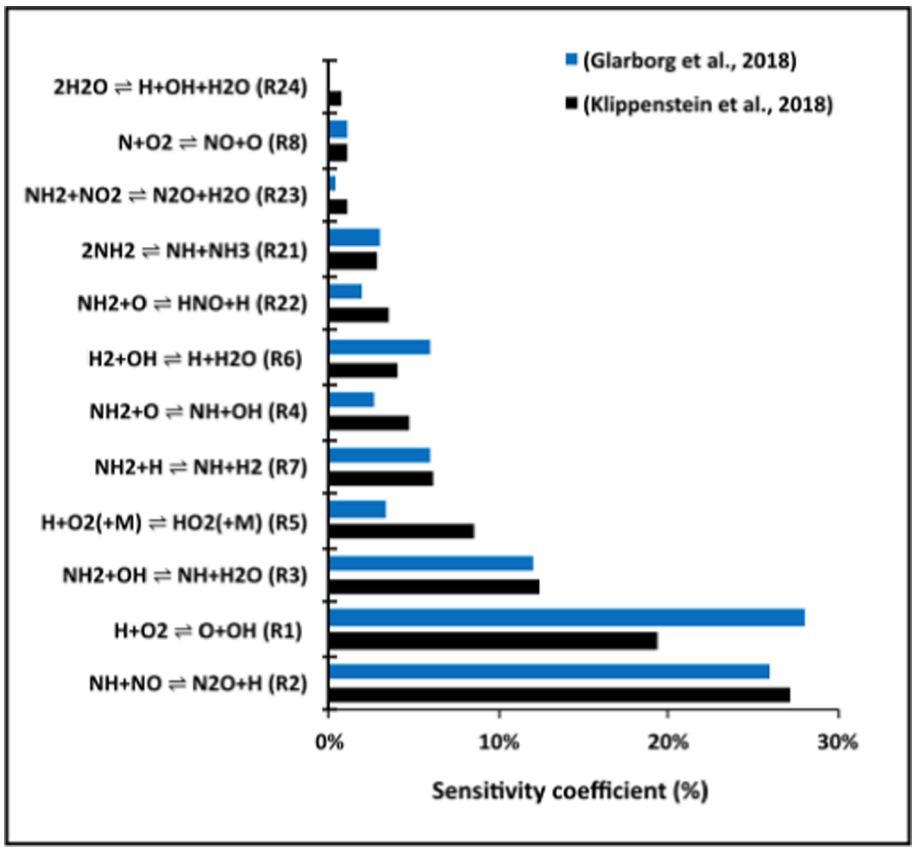

Fig. 8. Reactions with the largest positive sensitivity coefficients for N_2O mole fractions in 70/30 vol% NH_3/H_2 premixed flame at $\varphi = 0.6$ in the Klippenstein and Glarborg kinetic models.

promoting the reactivity of the system with O and OH radicals. Similarly, reaction steps R6 and $2NH_2 \rightleftharpoons NH + NH_3$ (**R21**) are also shown to have a high sensitivity coefficient value towards N_2O formation in Glarborg's model. In contrast, Klippenstein's model identifies key reactions R4, R5, $NH_2 + O \rightleftharpoons HNO + H$ (**R22**), and $NH_2 + NO_2 \rightleftharpoons N_2O + H_2O$ (**R23**) as having high values of positive sensitivity values, which suggests they are more effective in promoting N_2O formation compared to Glarborg's model. Additionally, Klippenstein's mechanism highlights the role of the key reaction $2H_2O \rightleftharpoons H + OH + H_2O$ (**R24**) in promoting N_2O formation, whereas this reaction's contribution is notably not observed in Glarborg's mechanism.

The chemistry of N_2O, for the key reactions that exhibit negative sensitivity coefficients towards N_2O mole fraction, is consistent across the selected kinetic models by Glarborg and Klippenstein, as illustrated in Fig. 9. Both models identify reaction steps R10, R11, R12, R16, R19 and R20 as having significant negative sensitivity coefficients, indicating their role in reducing the N_2O mole fraction. However, the trends of these reactions differ, highlighting mechanistic variations between the kinetic models in terms of rate parameters. Glarborg's model demonstrates a pronounced trend for the reaction steps R10, R11, and R12, in contrast to Klippenstein's model, which predicts a higher sensitivity coefficient for reaction step R19 than that in the Glarborg model. This further indicates differences in how each model approaches the N_2O consumption process.

The discrepancies in predictions among the kinetic models under consideration arise from mechanistic differences. A detailed comparative analysis of the models developed by Klippenstein and Glarborg reveals significant differences, particularly regarding rate parameter values and the definition of reaction steps. The rate parameters, crucial for the predictive accuracy of kinetic models, show notable variances between the two models. Specifically, the Klippenstein model utilizes distinct rate parameters for reaction steps identified in Table 4, such as $HO_2 + NH_2 \rightleftharpoons NH_3 + O_2$, $HO_2 + NH_2 \rightleftharpoons H_2NO + OH$, $HO_2 + NH_2 \rightleftharpoons H_2O + HNO$, and $N + O_2 \rightleftharpoons NO + O$, which significantly differ from those employed in the Glarborg model. These differences in rate parameters critically impact the model's ability to accurately simulate reaction kinetics and predict results.

The study by Klippenstein and Glarborg et al. [82] highlights the importance of the $NH_2 + HO_2$ reaction in the ignition and oxidation of NH_3 at high pressures and intermediate temperatures, emphasizing its product channels ($\rightarrow NH_3 + O_2$, $\rightarrow HNO + H_2O$, $\rightarrow H_2NO + OH$, and $\rightarrow NH_2OOH$). The pivotal role of the $HO_2 + NH_2$ reaction has also been supported by studies [63,83,84], indicating that calculations of ignition and oxidation at high pressures and intermediate temperatures are sensitive to the rate constant and branching ratio for $HO_2 + NH_2$. Moreover, the Klippenstein model outlines a reaction pathway, $H_2NO + HO_2 \rightleftharpoons H_2O_2 + HNO$, potentially involving unique intermediate species that are not directly included in the Glarborg model. Due to its significance in the hydrogen abstraction from H_2NO, this particular reaction plays a pivotal role in the combustion of ammonia, notably at lower temperatures [85].

These mechanistic differences, covering both rate parameter values and specific reaction steps reflect the discrepancies among the kinetic models in terms of laminar flame velocity and speciation mole fractions. The selection of rate parameters and the description of reaction pathways are instrumental in defining the model's predictive capabilities, emphasizing the need for thorough validation against experimental data. Consequently, the observed differences between the Klippenstein and Glarborg models not only illustrate the inherent challenges in kinetic modelling but also underscore the necessity for continuous refinement and experimental comparison to enhance model accuracy and reliability.

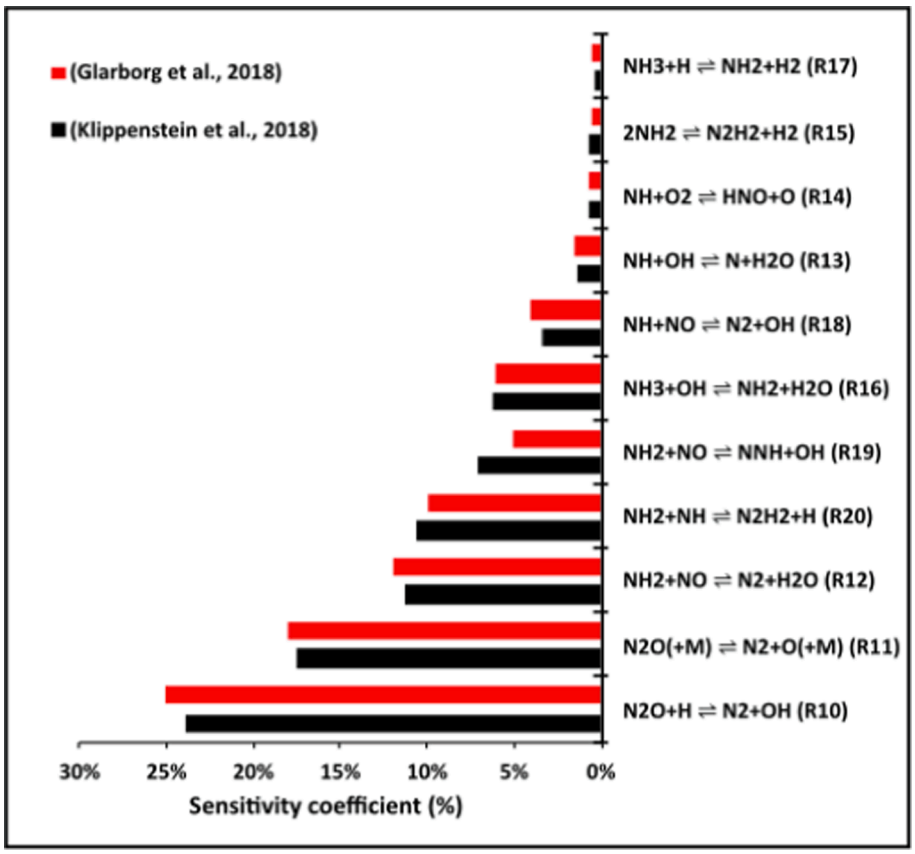

Fig. 9. Reactions with the largest negative sensitivity coefficients for N_2O mole fractions in 70/30 vol% NH_3/H_2 premixed flame at $\varphi = 0.6$ in the Klippenstein and Nakamura kinetic models.

Table 4
Key Reactions Illustrating Model Differences Between Klippenstein and Glarborg Kinetic Models.

Reactions	(Klippenstein et al., 2018)			(Glarborg et al., 2018)		
	A	**n**	**E**	**A**	**n**	**E**
$HO_2 + NH_2 \rightleftharpoons NH_3 + O_2$	1.70E+04	1.55	2027	1.5E+14	0	0
$HO_2 + NH_2 \rightleftharpoons H_2NO + OH$	2.50E+17	−1.28	1166	2.5E+13	0	0
$HO_2 + NH_2 \rightleftharpoons H_2O + HNO$ (DUPLICATE)	1.60E+07	0.55	525	2.5E+12	0	0
$HO_2 + NH_2 \rightleftharpoons H_2O + HNO$ (DUPLICATE)	5.70E+15	−1.12	707	–	–	–
$HO_2 + NH_2 \rightleftharpoons H_2O + HON$ (DUPLICATE)	2.10E+07	0.64	811	–	–	–
$N + O_2 \rightleftharpoons NO + O$	6.40E+09	1.00	6280	5.9E+09	1	6280
$H_2NO + HO_2 \rightleftharpoons H_2O_2 + HNO$	2.90E+04	2.69	−1600	Missing		

*Units are cm^3, mol, s, cal, K.

Fig. 10 and Fig. 11 show the variation of N_2O production and consumption rates as a function of distance, respectively, by the most important N_2O reactions in the Nakamura and the Klippenstein mechanisms. As can be noticed from Fig. 10 and Fig. 11, the net production rate of N_2O increases when the temperature of the system increases sharply and then this is followed by a sudden decrease downstream. According to Nakamura's kinetic model, the climbing influence of the total component of N_2O is governed by the action of reaction R2 which is responsible for 99 % of the N_2O formation in the combustion zone (see Fig. 12), while the decrease in N_2O is basically due to the retarding influence of reaction R10 which accounts for 85 % of the summed reaction rate of all N_2O consuming reactions (see Fig. 13). Similarly, Klippenstein's kinetic model shows an increase in the total N_2O due to the R2 reaction and then consumed by reactions R10 and R11, which thus are considered substantial in the consumption of N_2O (see Fig. 13).

The chemical pathways presented in Fig. 14 also show the dominant role of reaction R2 in the formation of N_2O, which indicates the dominant role of NH radicals in the production of N_2O (i.e. accounts for almost 98 %), as well as the substantial part of reaction R10 in the consumption of N_2O, which leads to production of N_2 and OH.

Fig. 13 shows different trends among the chosen mechanisms. The Nakamura kinetic model shows a higher level of N_2O consumption by reaction R10 when compared to the Klippenstein model. Conversely, the Klippenstein model shows increased consumption rates for reactions R11, $N_2O + O \rightleftharpoons 2NO$ (**R25**), $N_2O + O \rightleftharpoons N_2 + O_2$ (**R26**), and $N_2H_2 + NO \rightleftharpoons N_2O + NH_2$ (**R27**) relative to those in the Nakamura model. Notably, reaction R27 has a negligible impact within the Nakamura mechanism. These differences in reaction sensitivities can be attributed to the variations in the rate parameters that control the reactions within each mechanism (see Table 3), which affect the rate of the selected reaction (see Fig. 15). As noticed from Fig. 15the Heat Release Rate (HRR) predicted by Klippenstein is greater than that estimated by Nakamura's model.

Fig. 10 and Fig. 11 also depict some insights that are quite significant. According to the study by Alnasif et al. [86], the laminar flame speed for the Klippenstein model (8.66 cm/s) is higher than that predicted by the Nakamura model (6.72 cm/s). This aligns with the well-known behaviour of stagnation flames, where the flame location is closely related to the flame speed. Faster flames usually stabilize closer to the inlet in areas with higher gas velocity. This is clearly shown in Fig. 10 and Fig. 11, where the flame, according to the Klippenstein model, is seen closer to the burner nozzle, while the Nakamura model, which has a slower flame speed, shows the flame stabilizing further from

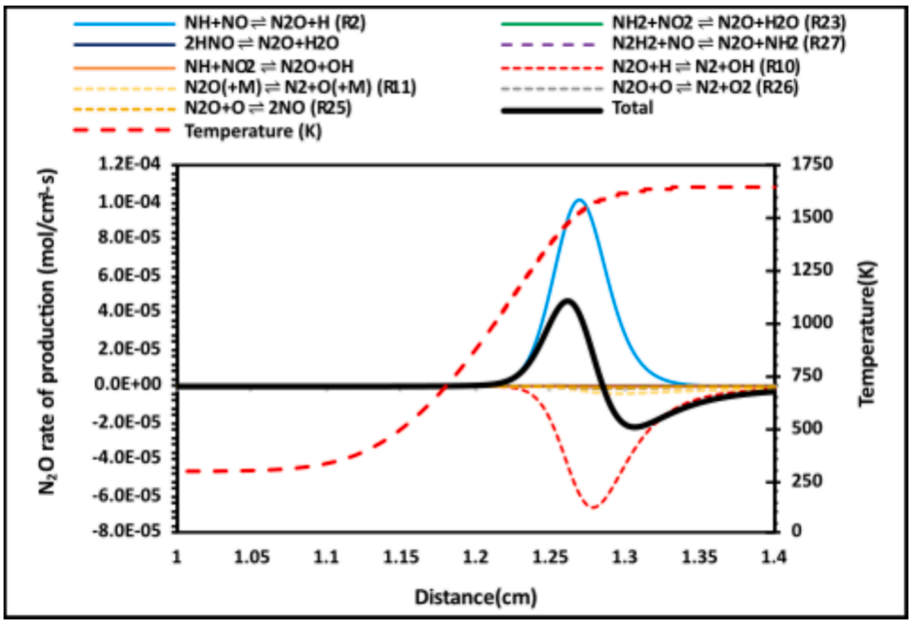

Fig. 10. The rate of production/consumption of N_2O for 70/30 vol% NH_3/H_2 mixture at 0.6 of ϕ estimated by the Nakamura mechanism.

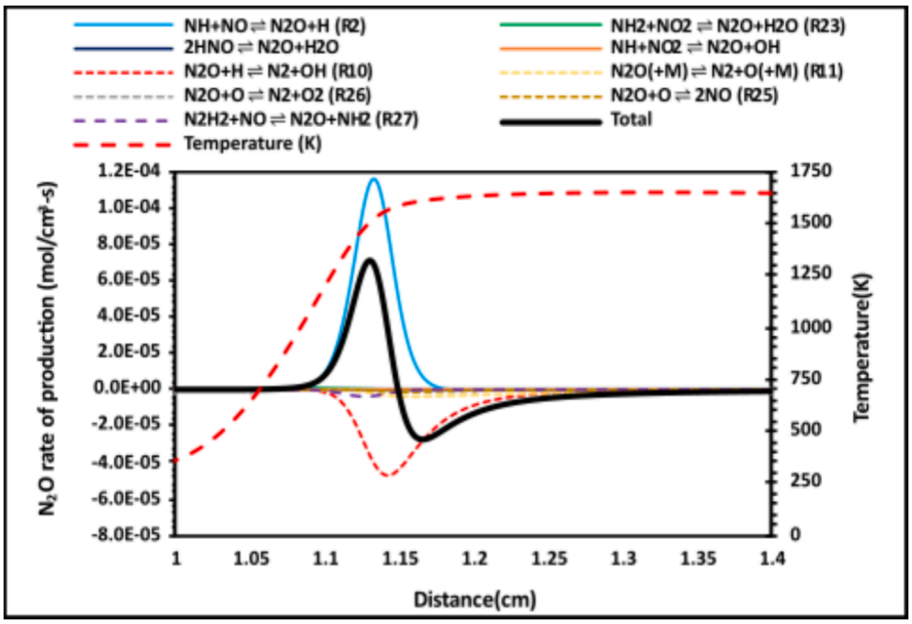

Fig. 11. The rate of production/consumption of N_2O for 70/30 vol% NH_3/H_2 mixture at 0.6 of ϕ estimated by Klippenstein kinetic model.

the nozzle.

The consumption behaviour of reaction R27 can be explained by the negative trend in the reaction rate of the aforementioned reaction, as shown in Fig. 15. Chemical reactions can shift their equilibrium position based on changes in temperature or the concentrations of reactants and products. A change in temperature, the depletion of a reactant, and the high concentration of products create conditions favourable for the dominance of the reverse reaction ($N_2O + NH_2 \rightarrow N_2H_2 + NO$), where the products react to form the reactants, resulting in an increase in reactant concentrations. This behaviour is clearly observable at 0 cm, as depicted in Fig. 16, where the mole fraction of N_2H_2 gradually increases while the concentration of NH_2 decreases.

The intensity rate of the reaction R27 increases when moving downstream, Fig. 15. According to the Klippenstein model, the reaction step R27 shows a pronounced temperature dependency (refer to Table 3). The rate of this reaction increases significantly with an increase in temperature, resulting in a marked decrease in the NH_2 mole fraction, as evidenced in Fig. 16, through the reverse reaction ($N_2O + NH_2 \rightarrow N_2H_2 + NO$). As the reaction progresses, reactants, particularly NH_2, are consumed, resulting in a deceleration of the reaction. As R27 demonstrates a minor impact on the depletion of N_2O, its influence appears to be potentially overstated in the Klippenstein model. The recent study by Cornell et al. [87] found that the original rate constant of R27 overestimates the mole fraction of N_2O, suggesting that this reaction is either too slow or has no significant impact on the N_2O mole fraction. Furthermore, the study observed that models with and without the inclusion of R27 showed nearly identical predictions. This indicates that the experimental datasets used for validation may not have adequately tested this specific reaction (see Section 3.4).

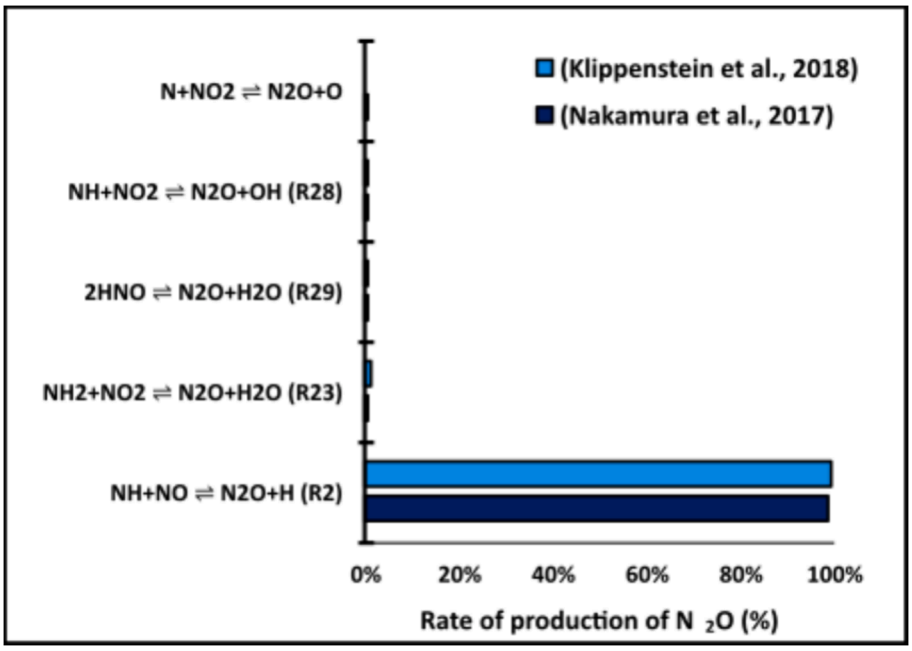

Fig. 12. Rate of production (in %) at $\varphi = 0.6$ estimated by the Nakamura and Klippenstein kinetic models.

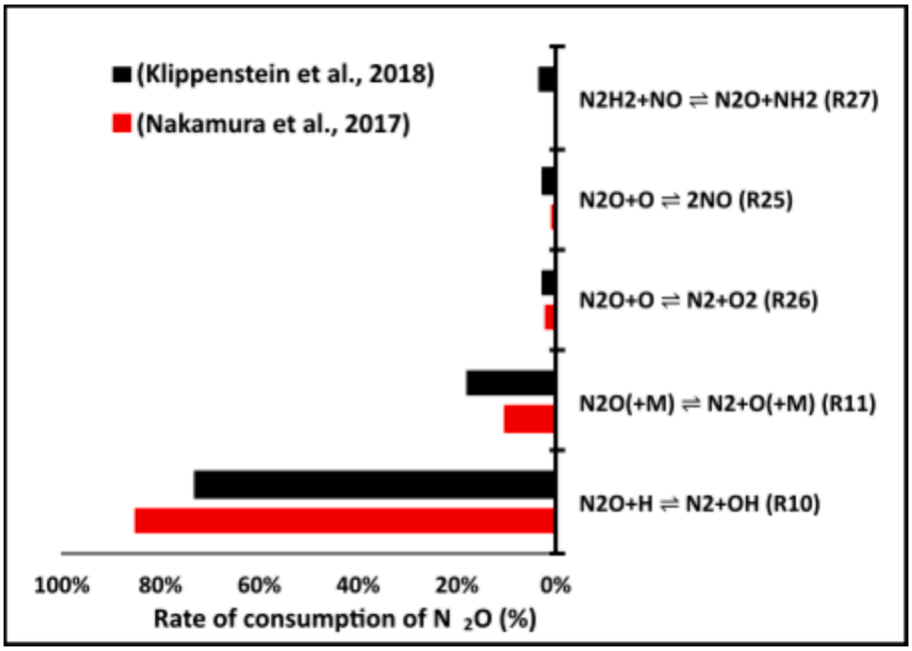

Fig. 13. Rate of consumption (in %) at $\varphi = 0.6$ estimated by the Nakamura and Klippenstein kinetic models.

3.2. Stoichiometric flame conditions

Based on Fig. 3, it has been observed that the mole fraction of N_2O has slightly increased. According to the normalised error results, the prediction accuracy of most tested mechanisms falls within the range of experimental uncertainty (Normalised error < 1). This indicates that a larger difference between the experimental and theoretical values is not significant, given the large uncertainty. Particularly at stoichiometric conditions for N_2O mole fraction, the magnitude of uncertainty exceeds the measured values, rendering the differences between simulations and experiments statistically insignificant and within the expected variability of the measurements. Consequently, the majority of the tested kinetic models demonstrate good performance in predicting N_2O mole fractions, as shown in Fig. 2.

Considering the uncertainty of the measurements, the estimation accuracy of the Klippenstein kinetic model falls within the range of the experimental value (normalised error less than 1), as depicted in Fig. 2. Furthermore, as observed from Fig. 2, the Zhang kinetic model [59] exhibits better performance, as its normalised error is lower than that of the Klippenstein model. Therefore, both the Klippenstein and Zhang reaction mechanisms will be analysed in terms of their behaviour in estimating N_2O, and the reasons behind their discrepancies in this condition will be explored.

Fig. 17 and Fig. 18 show the most influential reactions on N_2O mole fractions with positive and the negative sensitivity coefficients estimated by Zhang and Klippenstein kinetic mechanisms, respectively. As

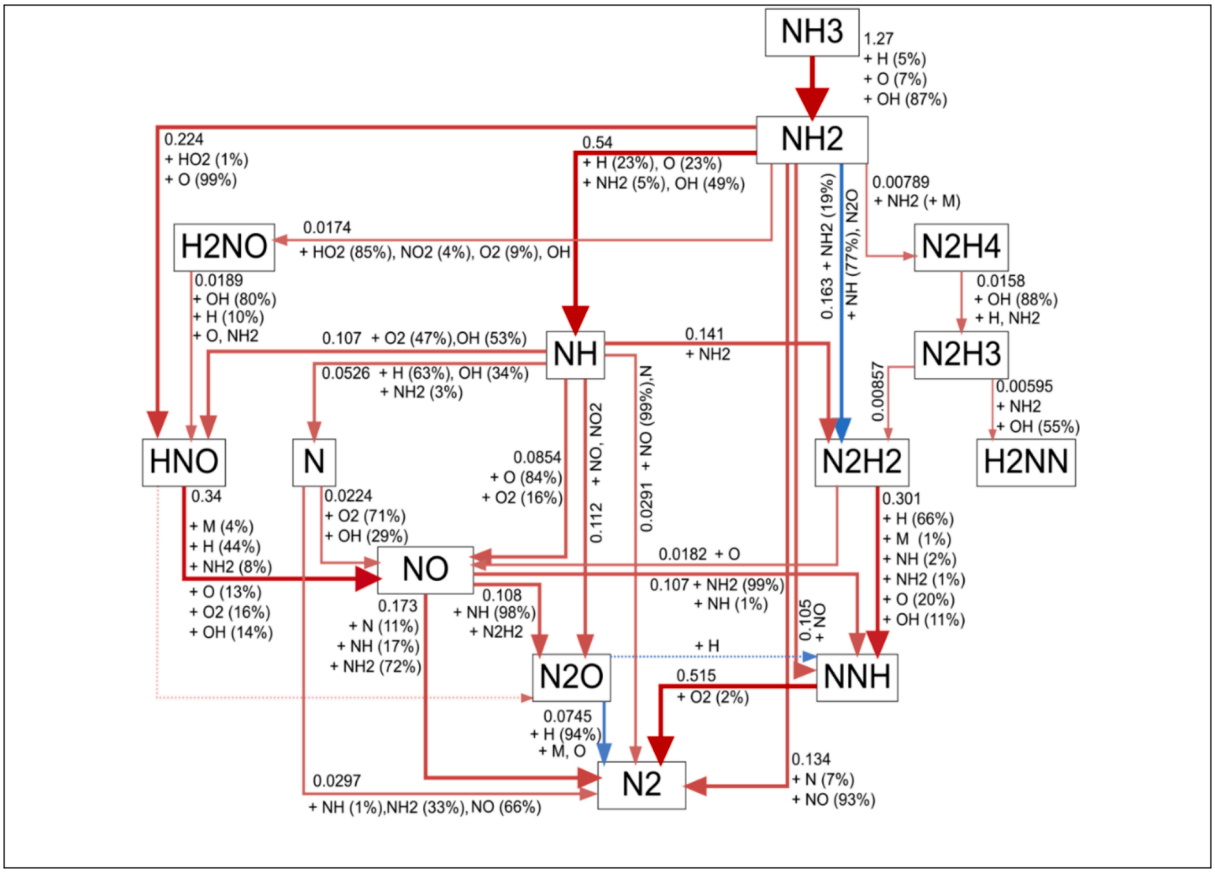

Fig. 14. Chemical reaction pathways of N_2O formation/consumption at flame zone ($T = 1498$ K) and at $\varphi = 0.6$ predicted by the Klippenstein model. Arrow lines refer to chemical transformations, percentages (%) show to the contribution of a reactant to the transformation, numbers stand for the net reaction rate in kmol/m^3s, which is also visualized by line thickness.

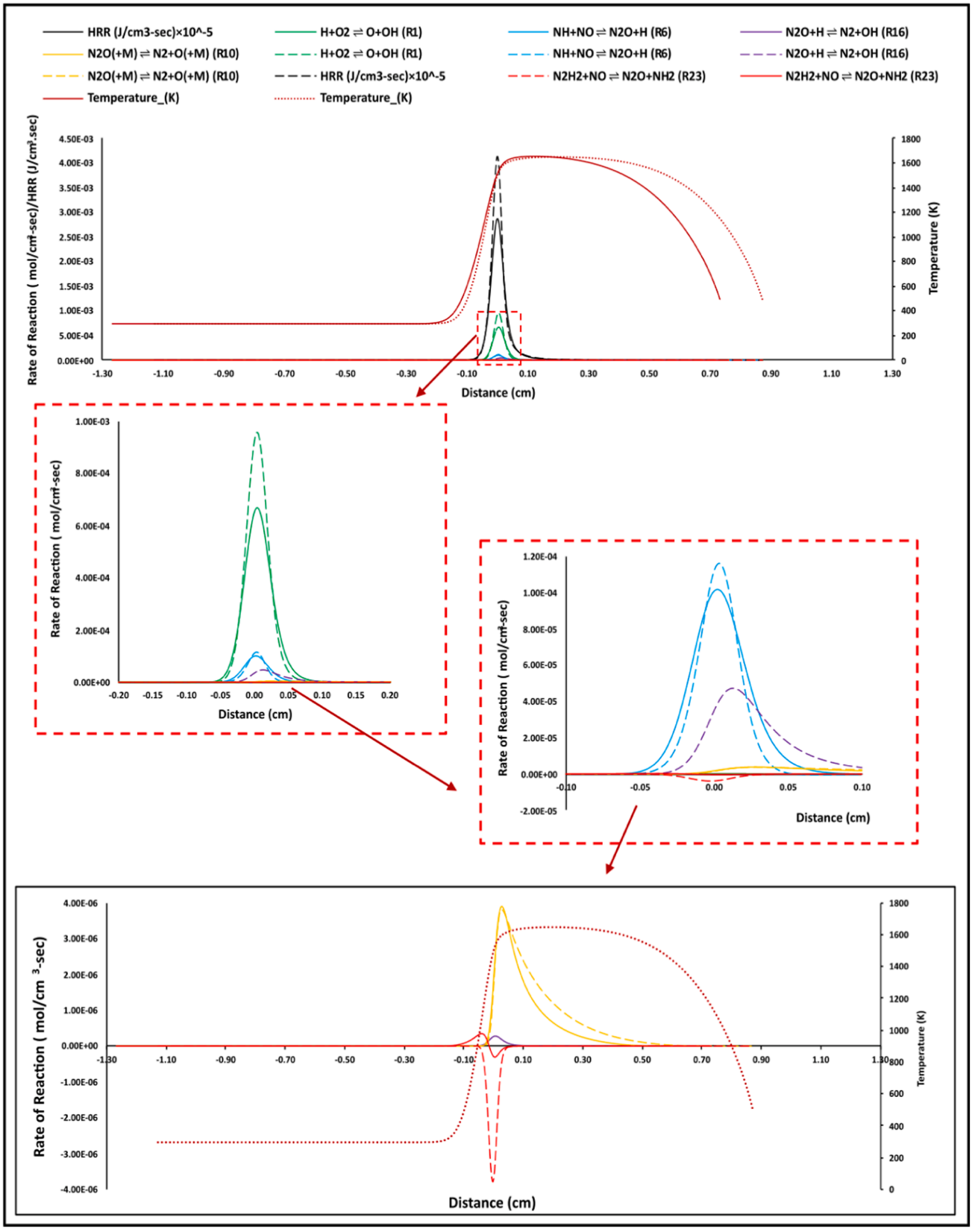

Fig. 15. The reaction rate profiles of reactions most influential to the formation/reduction of N_2O mole fractions for 70/30 vol% NH_3/H_2 mixture at $\varphi = 0.6$. The result for the Nakamura and Klippenstein kinetic models is shown with solid and dashed lines, respectively.

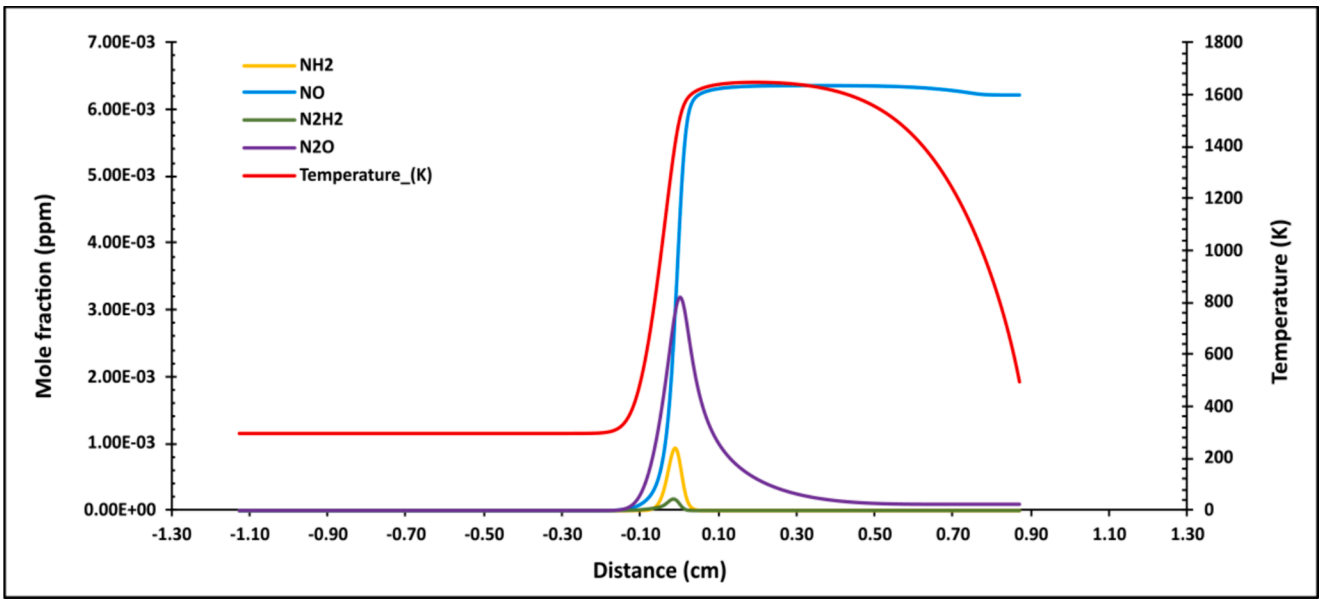

Fig. 16. Variation of NH_2, NO, N_2H_2, and N_2O mole fractions, as well as temperature, as a function of axial distance in a 70/30 vol% NH_3/H_2 mixture at $\varphi = 0.6$, as predicted by the Klippenstein kinetic model.

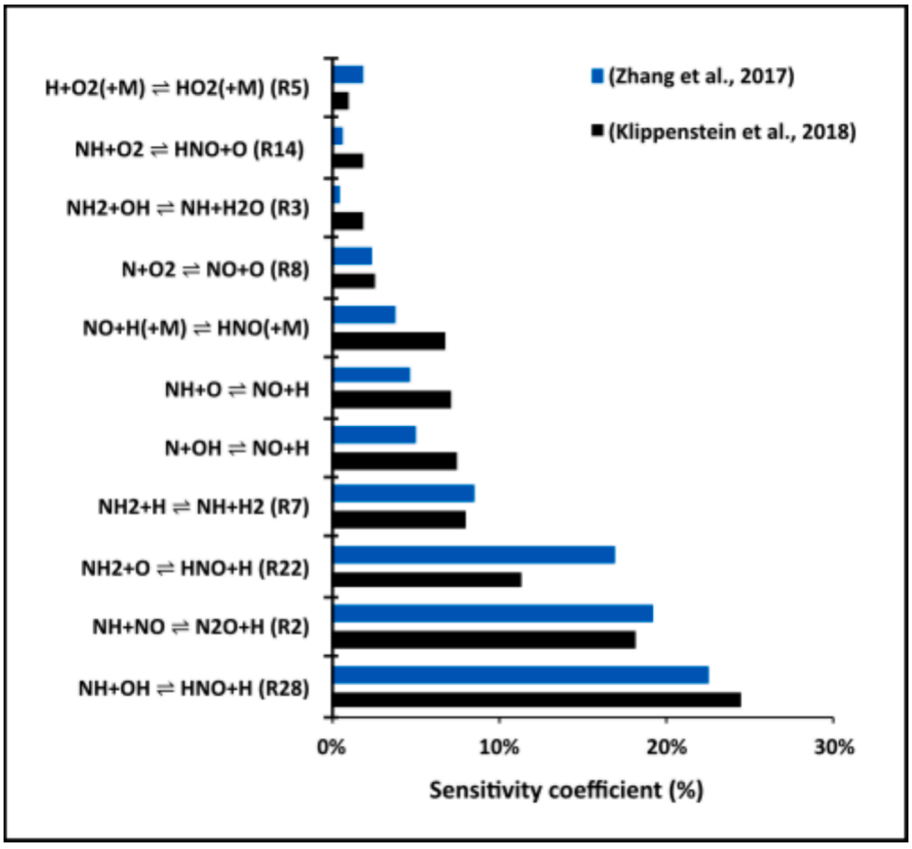

Fig. 17. Reactions with the largest positive local sensitivity coefficients for N_2O mole fractions in 70/30 NH_3H_2 vol% premixed flame at $\varphi = 1$ in the Klippenstein and Zhang kinetic models.

shown in Fig. 17, both kinetic models indicate the same reaction steps having a positive impact on N_2O formation, though with different trends in sensitivity values. In both models, the reactions $NH + OH \rightleftharpoons HNO + H$ (**R28**) R2, R7, and R22 are identified as the most dominant in increasing the mole fraction of N_2O by enhancing the H and H_2 pools within the system, thus improving system reactivity. Klippenstein's model displays a higher sensitivity trend for the reaction R28 compared to the Zhang model, which, conversely, shows higher sensitivity values for reactions R2, R7, and R22 for N_2O formation. The variation in their sensitivity values is due to the different values of their rate parameters among the selected models, which in turn control their reaction rates. According to Fig. 18, both models indicate the highest negative sensitivity coefficient

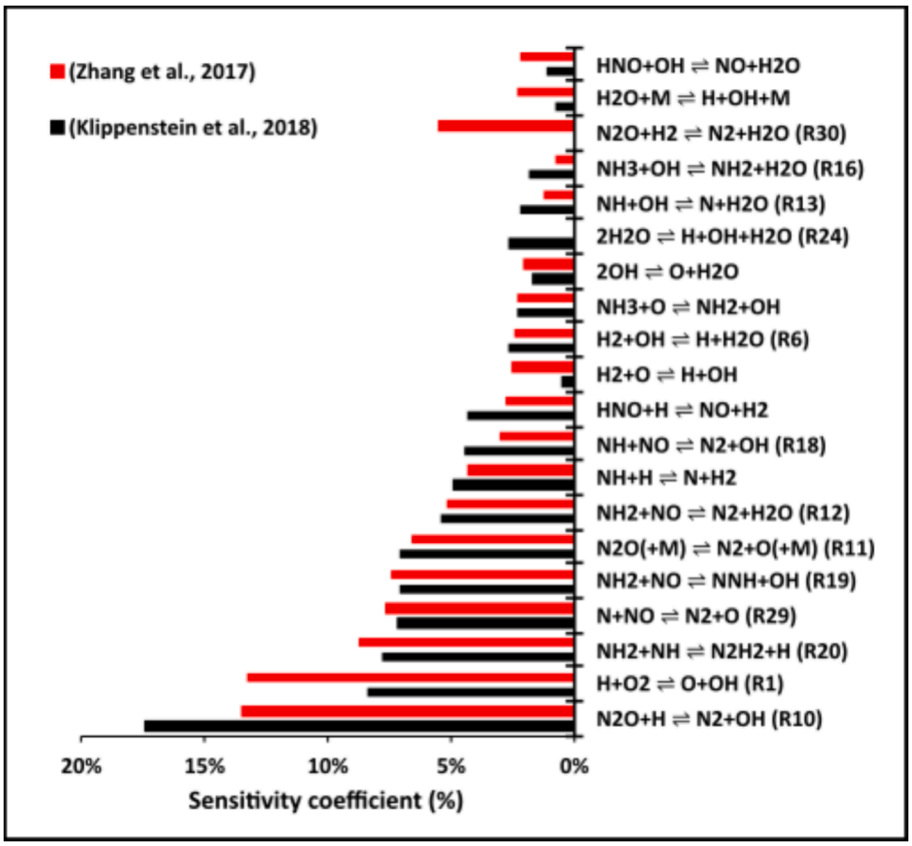

Fig. 18. Reactions with the largest negative local sensitivity coefficients for N_2O mole fractions in 70/30 NH_3H_2 vol% premixed flame at $\varphi = 1$ in the Klippenstein and Zhang kinetic models.

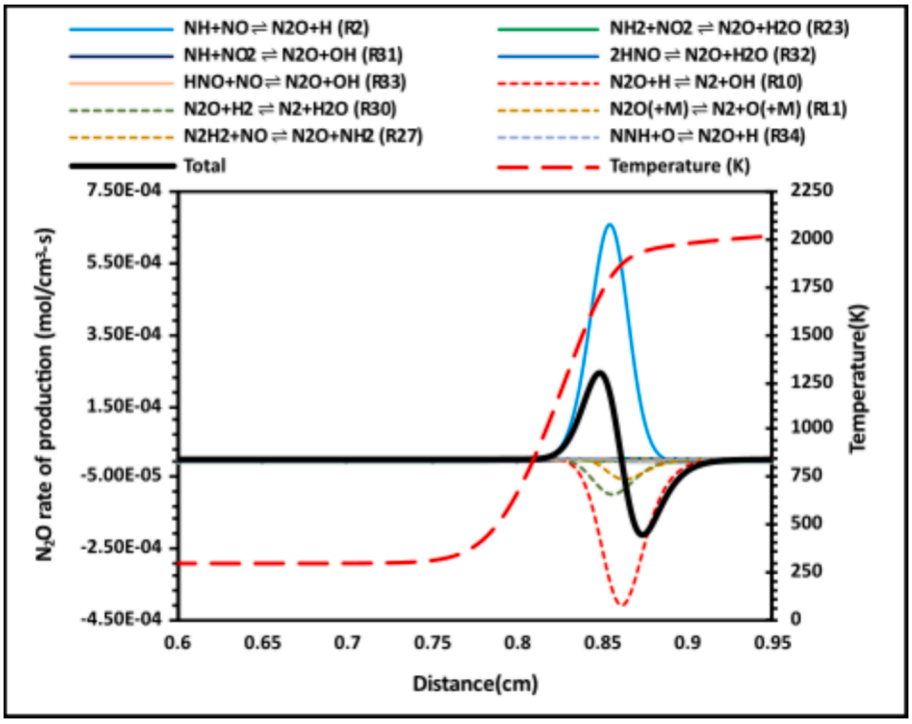

Fig. 19. The rate of production/consumption of N_2O in 70/30 vol% NH_3/H_2 mixture at stoichiometric conditions by the model of Zhang.

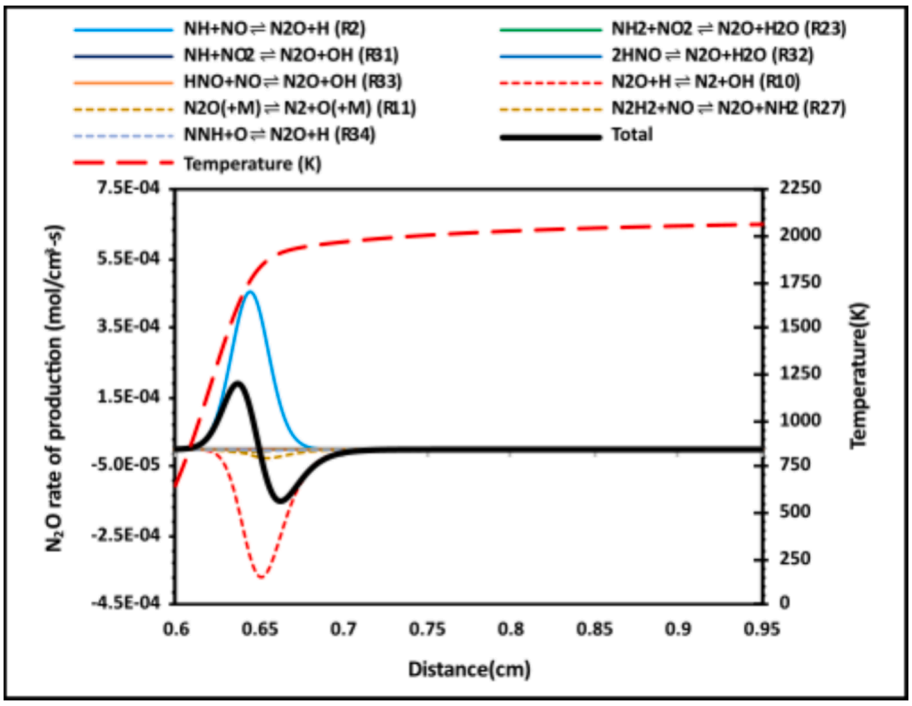

Fig. 20. The N_2O rate of production/consumption in 70/30 vol% NH_3/H_2 mixture at stoichiometric conditions by the Klippenstein kinetic model.

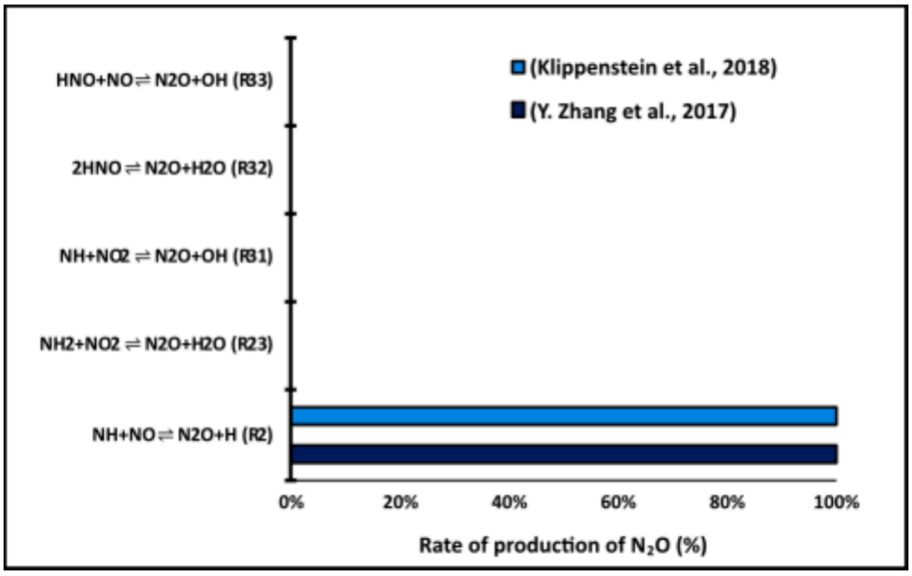

Fig. 21. Rate of production at stoichiometric conditions estimated by the Zhang and Klippenstein kinetic models.

for reaction R10 (Klippenstein: 17 %, Zhang: 14 %), making this reaction the most significant in slowing N_2O formation. Additionally, reactions R11 and R12 display slightly higher values in the Klippenstein model compared to the Zhang model. In contrast, the Zhang kinetic model predicts higher negative sensitivity trends for the reaction steps R1, R19, R20, $N + NO \rightleftharpoons N_2 + O$ (**R29**) than the Klippenstein model. Furthermore, the reaction step $N_2O + H_2 \rightleftharpoons N_2 + H_2O$ (**R30**), which contributes to an increase in the N_2O consumption in the Zhang mechanism, does not have an effect on the Klippenstein mechanism. Instead, Klippenstein's model emphasizes the role of reaction step R24 in inhibiting N_2O formation.

Fig. 19 and Fig. 20 showcase the rate distribution for the formation and consumption of N_2O across the computational domain, as determined by the kinetic reaction mechanisms of Zhang and Klippenstein, respectively. The Figures clearly demonstrate that the total concentration of N_2O initially rises, mainly due to the N_2O-forming reaction R2. Other reactions, such as R23, $NH + NO_2 \rightleftharpoons N_2O + OH$ (**R31**), $2HNO \rightleftharpoons N_2O + H_2O$ (**R32**), and $HNO + NO \rightleftharpoons N_2O + OH$ (**R33**), contribute less significantly to the increase of the N_2O mole fraction in both models (see Fig. 21). Unlike R2, which has a low activation energy R32, and R33 exhibit slower reaction rates due to higher activation energies, acting as barriers to N_2O formation. This occurs because the reactants are consumed more readily by other reactions that require lower activation energy. This pattern is evident in both kinetic models, as illustrated in Fig. 19. On the other hand, the reduction in the total N_2O concentration is due to the consumption effects of reactions R10, R11, R27, R30, and

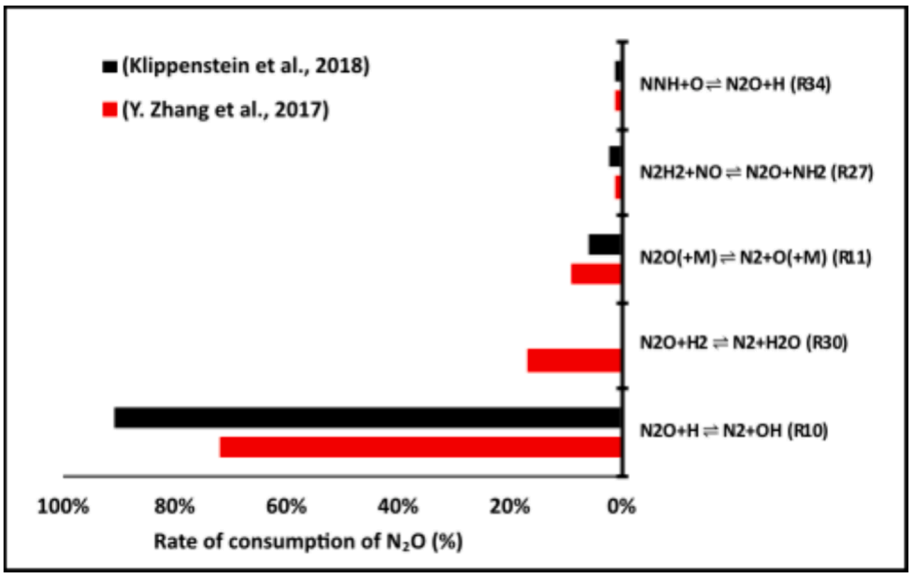

Fig. 22. Rate of consumption at stoichiometric conditions estimated by the Zhang and Klippenstein kinetic models.

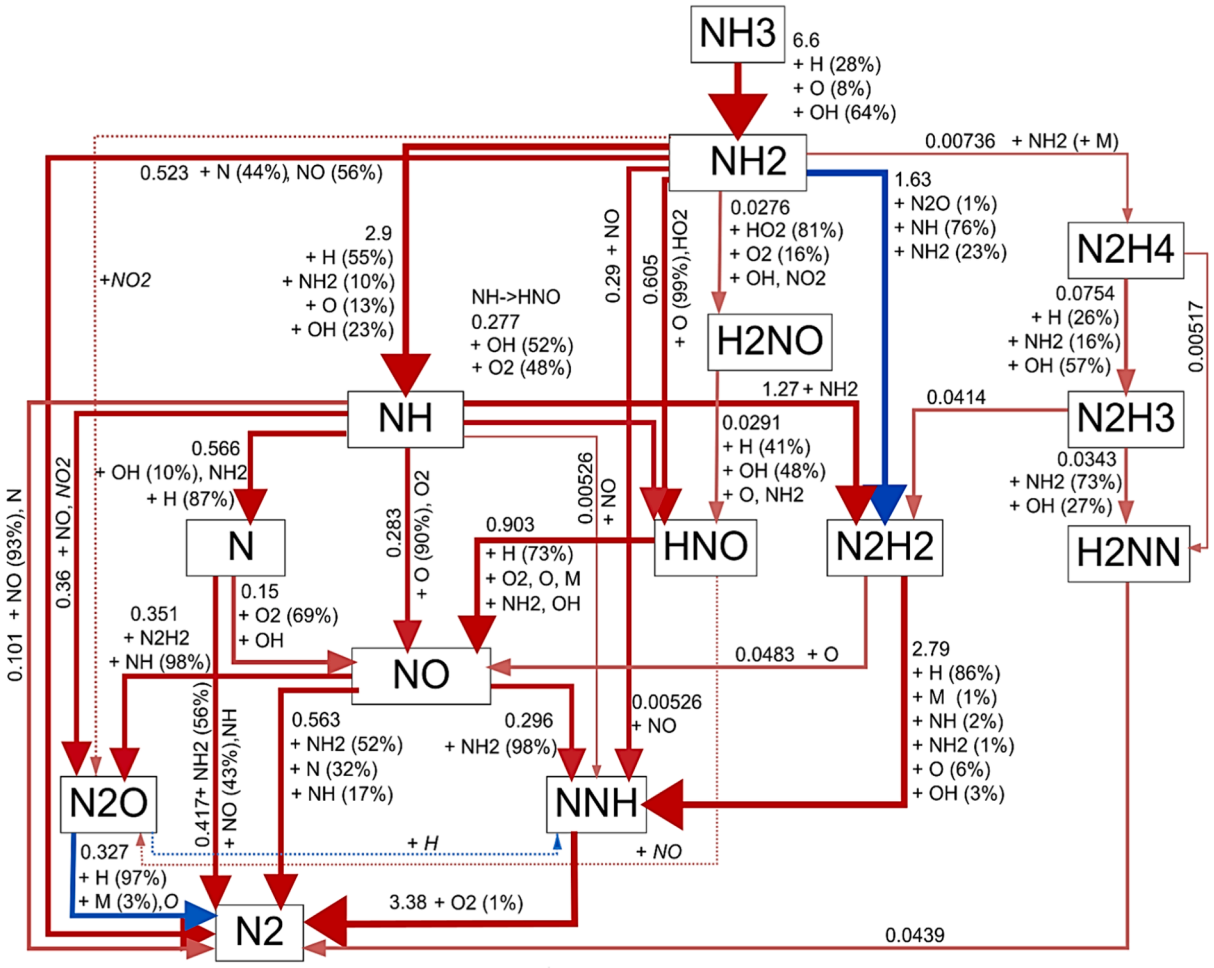

Fig. 23. Chemical reaction pathways of N_2O formation/consumption at flame zone ($T = 1619$ K) and at $\varphi = 1$ predicted by the Klippenstein model. Arrow lines refer to chemical transformations, percentages (%) refer to the contribution of reactants to the transformation, numbers stand for the net reaction rate in kmol/m^{3}s, which is also visualized by line thickness.

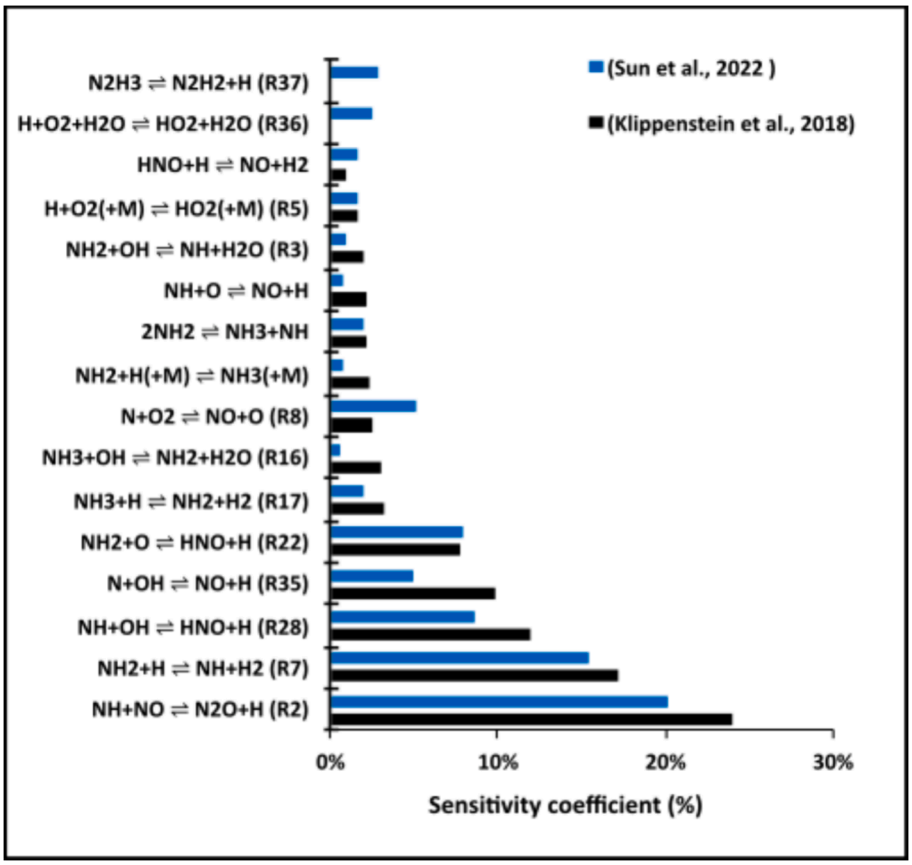

Fig. 24. Reactions with the largest positive local sensitivity coefficients for N_2O mole fraction in 70 NH_3/30 H_2 vol% premixed flame at $\varphi = 1.4$ in the Klippenstein and Sun kinetic models.

NNH + O ⇌ N_2O + H (**R34**), as indicated in Fig. 22. Additionally, within the Zhang mechanism, reaction R30 is identified as the second most significant reaction in reducing N_2O formation, a reaction not observed in the Klippenstein mechanism (see Fig. 22). Furthermore, the rate of N_2O consumption in reaction R11 is higher in the Zhang model compared to the Klippenstein kinetic model, which, in contrast, predicts higher consumption rates for reactions R10 and R27.

Fig. 19 and Fig. 20 also show that the Klippenstein model stabilizes the flame closer to the burner, with a flame speed of 27.62 cm/s, compared to the Zhang model, which has a flame speed of 21.38 cm/s [82].

Fig. 23 illustrates the main pathways for the formation/ consumption of N_2O in terms of net reaction rate in the reaction zone where T = 1619 K. As shown in the figure, formation of N_2O from NO occurs mainly (in 98 %) via reaction with NH radicals according to R2, as well as dashed pathways: $NH_2 + NO_2 \rightleftharpoons N_2O + H_2O$ (**R23**) and HNO + NO ⇌ N_2O + OH (**R33**) also contribute to the formation of N_2O. On the other hand, the chemical pathways for the consumption of N_2O shows that N_2O decomposes almost exclusively (in 99 %) into N_2 by reacting with H atoms in reaction R10 (~0.97 × 99 % = 96 %) and by unimolecular decay in R11 (~3 %), whereas the remaining 1 % of N_2O is consumed by reaction R26.

3.3. Rich flame conditions

The mole fraction of N_2O starts decreasing when the equivalence ratio increases to rich conditions and become close to zero at $\varphi = 1.4$ (see Fig. 3). In the rich range, the uncertainty values are large and exceed the experimental values of N_2O. This leads to statistically insignificant differences between simulations and experiments, falling within the expected variability of the measurements. The high magnitude of uncertainty in rich conditions reflect the accuracy of most of the tested mechanisms in this range, as most of the kinetic models have a normalised error of less than 1. This indicates that the N_2O mole fractions predicted by most of the simulated kinetic models are within the error range of the experimental measurements. At an equivalence ratio (φ) of 1.4, the kinetic model of Klippenstein, which predicted the N_2O mole fraction, was within the error range (normalised error = 0.025). At the same time, several reaction mechanisms showed superior performance in the estimation of N_2O, such as the Sun kinetic model [47], which recorded a normalised error of 0.001 based on the experimental measurements, considering uncertainty. Therefore, both Klippenstein's and Sun's kinetic reaction mechanisms will be analysed in terms of sensitivity and rate of formation/consumption of N_2O to examine the reasons behind their discrepancies under these conditions.

As shown in Fig. 24, the N_2O mole fraction can be extremely boosted by the action of the reactions R2, R7, R22, R28 and N + OH ⇌ NO + H (**R35**). These Reactions are responsible for increasing the system reactivity by increasing the H and NH pools. It should be highlighted that reaction steps $H + O_2 + H_2O \rightleftharpoons HO_2 + H_2O$ (**R36**) and $N_2H_3 \rightleftharpoons N_2H_2 + H$ (**R37**) have no influence on the N_2O mole fraction in the Klippenstein mechanism, while they play a role in promoting N_2O formation in the mechanism of Sun. Fig. 25 illustrates that reactions R1, R10, R11, R12, R19, R20, and R29 have a considerable effect on reducing the concentration of N_2O by consuming H, NO, and NH species. Although both kinetic models show nearly the same reactions which have positive/ negative trends on N_2O concentration, the estimated figures in most cases are different for the two mechanisms.

As shown in Fig. 26 and Fig. 27, the increasing trend of the total N_2O can be explained by the increasing rate of the N_2O producing R2 reaction. Furthermore, both selected kinetic models give the same estimation for the N_2O-production rate of reaction R2 (see Fig. 28). Meanwhile,

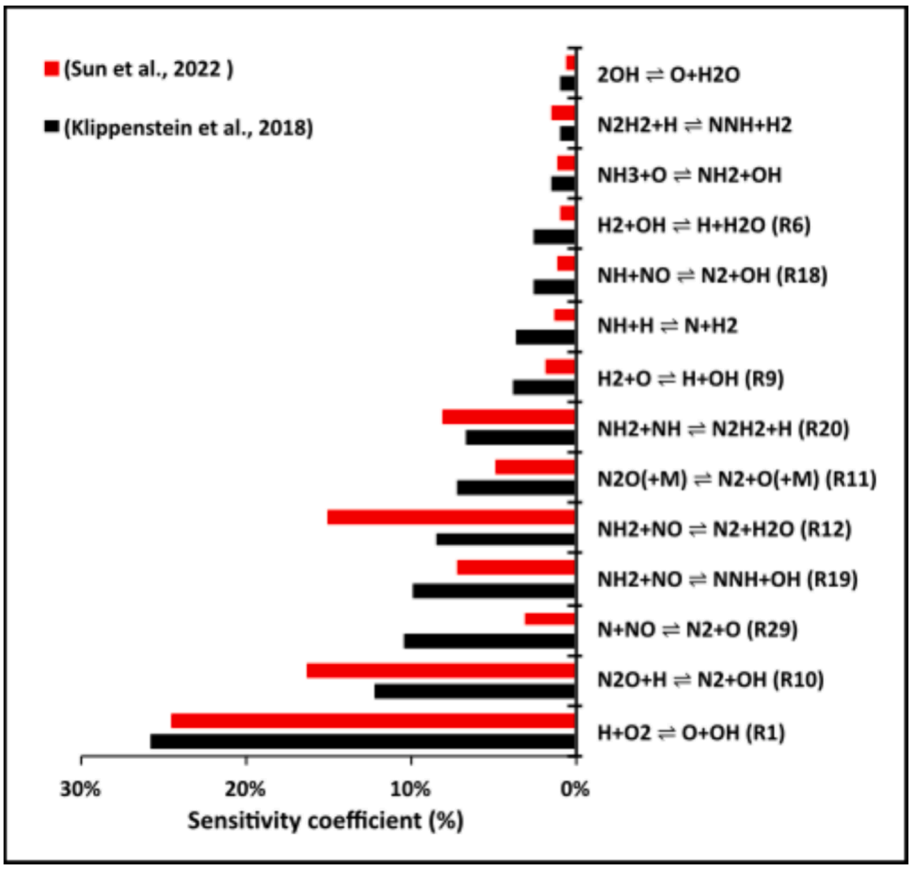

Fig. 25. Reactions with the largest negative local sensitivity coefficients for N_2O concentration in 70/30 vol% NH_3/H_2 premixed flame at $\varphi = 1.4$ in the Klippenstein and Sun kinetic models.

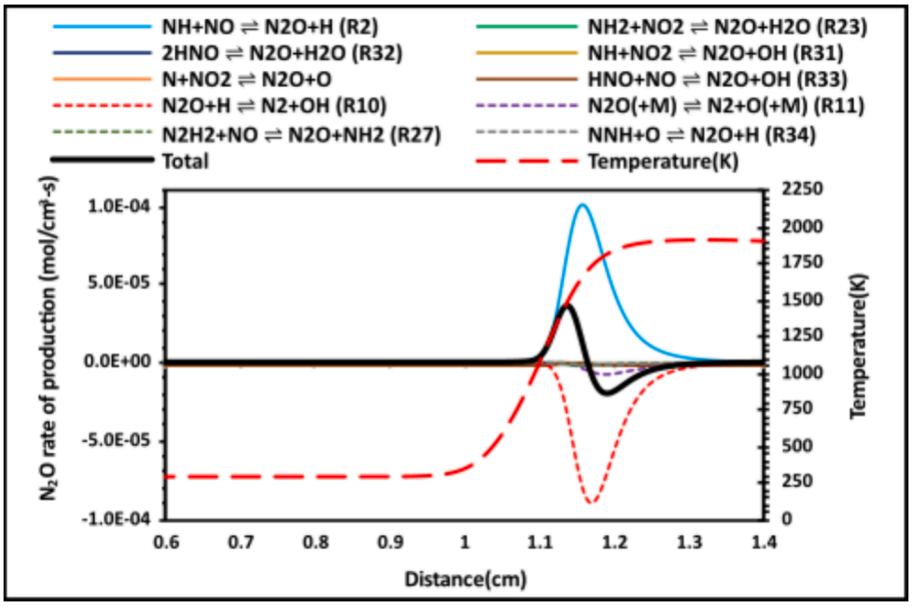

Fig. 26. The rate of production/consumption of N_2O in 70/30 vol% NH_3/H_2 mixture at $\varphi = 1.4$ estimated by the Sun kinetic model.

the peaking rates of N_2O consuming reactions R10 and R11 cause the sharp decrease in the total rate of N_2O concentration change. In addition, the rate of reaction R10 estimated by the Klippenstein kinetic model is slightly lower than that of Sun's reaction model (Fig. 29). Additionally, in rich conditions, despite both chosen models predicting nearly identical N_2O mole fractions, their predicted flame locations also differ. The Klippenstein model predicts a flame location close to the inlet, suggesting a faster flame that stabilizes near the inlet, Fig. 27 In contrast, the Sun kinetic model indicates a slower flame, stabilizing further away from the inlet, Fig. 26.

It has been also observed the dominant role of the reaction R2 in increasing N_2O concentration, as well as the negative influence of

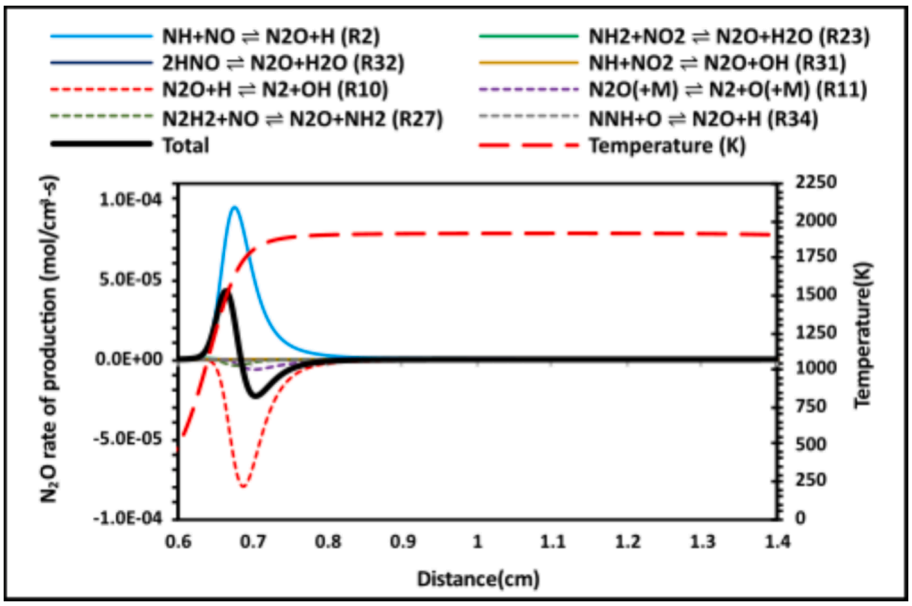

Fig. 27. The rate of production/consumption of N_2O in 70/30 vol% NH_3/H_2 mixture at $\varphi = 1.4$ estimated by the Klippenstein model.

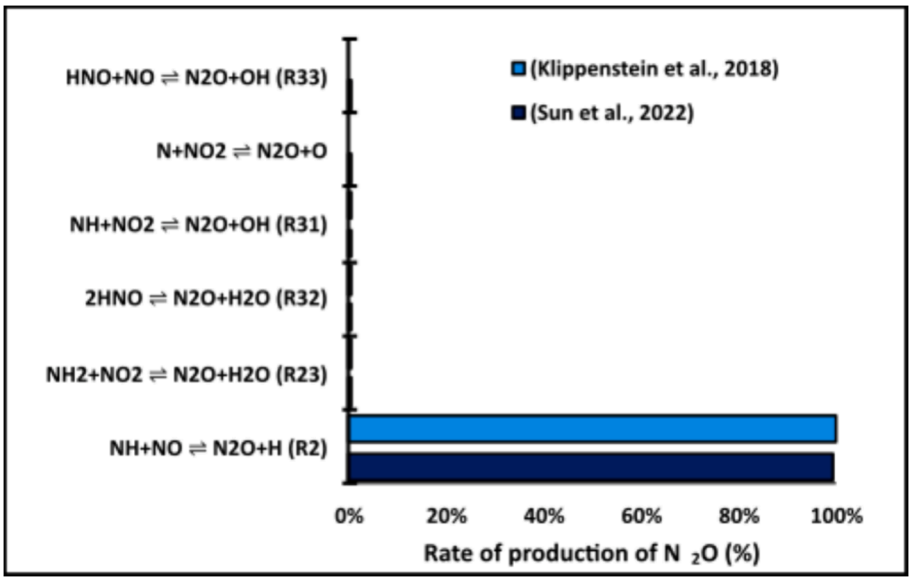

Fig. 28. Rate of production of N_2O at $\varphi = 1.4$ estimated by the Sun and Klippenstein kinetic models.

reactions R10 and R11 on the consumption of N_2O at rich conditions can be seen clearly in the pathway diagram in Fig. 30. The diagram shows the rates at 1478 K, which corresponds to the peak value of the total N_2O production rate. The pathway diagram shows that reaction NH + NO ⇌ N_2O + H (**R2**) accounts for about 98 % of the NO to N_2O transformation. Further, reaction N_2O + H ⇌ N_2 + OH (**R10**) is responsible in 98 % for the decomposition of N_2O to N_2, and the formation of N_2H_2 from NH_2 takes place in 23 % via reaction N_2H_2 + NO ⇌ N_2O + NH_2 (**R27**) (see blue lines in Fig. 30).

From the previous sections, the investigation of the performance of tested kinetic models under different conditions of φ by Klippenstein et al. [56], Glarborg et al. [50], Nakamura et al., Zhang et al. [18], and Sun et al. [47] demonstrated that kinematic differences among the mechanisms are the reason for the discrepancies in the predictions of the selected mechanisms. Additionally, the good performance of the kinetic models in specific conditions does not necessarily reflect their accuracy in predicting N_2O concentration.

The kinematic differences of the key reactions H_2 + N_2O ⇌ H_2O + N_2, N_2O + M ⇌ N_2 + O + M, and N_2O + NH_2 ⇌ NO + N_2H_2 among the kinetic models are clearly depicted in Fig. 31. According to the rate production analysis at stoichiometric conditions, the key reaction H_2 + N_2O ⇌ H_2O + N_2 shows high values which significantly impacts N_2O consumption in the Zhang kinetic model. In contrast, it shows no effect in the kinetic models of Klippenstein, Nakamura, Sun, and Glarborg, indicating that the actual rate of this reaction is much lower as proved by Mulvihill et al. [88].

Similarly, the key reaction N_2O + NH_2 ⇌ NO + N_2H_2 shows nearly the same rate constant in the tested kinetic models of Klippenstein, Zhang, Sun, and Glarborg, indicating a similar effect on the consumption of N_2O concentration. Only Nakamura's model shows a different trend. Meanwhile, the study by Cornell et al. [87] has shown that the rate constant of the reaction N_2O + NH_2 ⇌ NO + N_2H_2 is likely over-estimated in the tested kinetic models and should be reduced by a factor of 10, Fig. 31 (b).

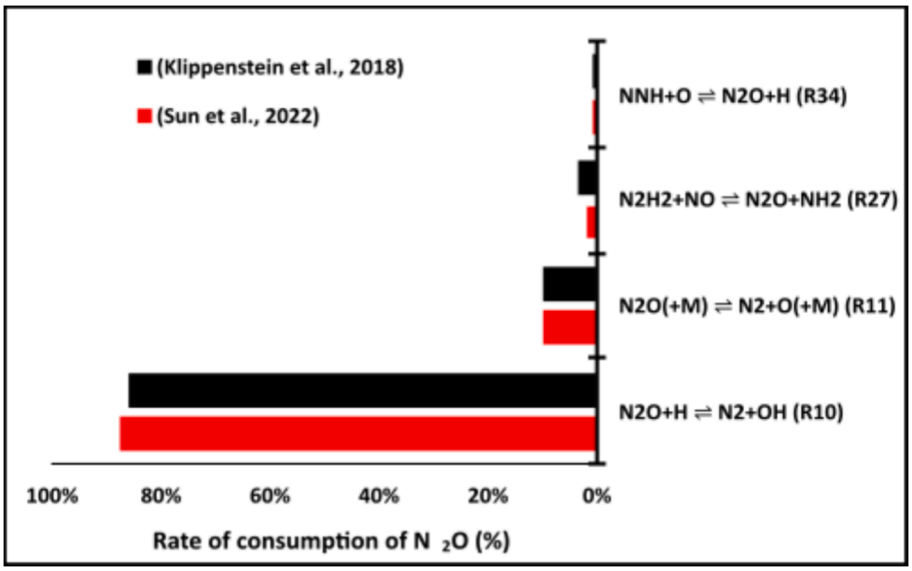

Fig. 29. Rate of consumption of N_2O at $\varphi = 1.4$ estimated by the Sun and Klippenstein kinetic models.

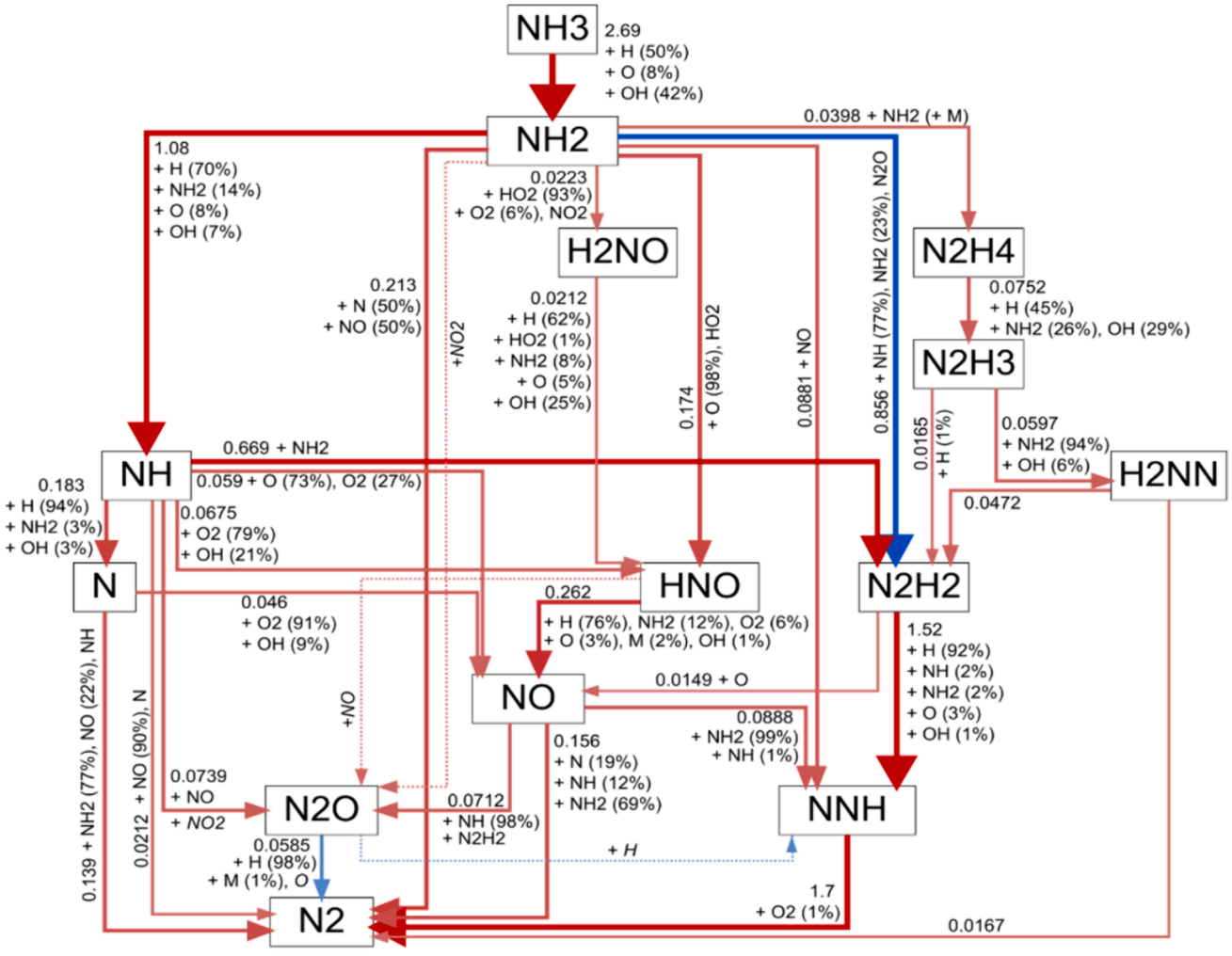

Fig. 30. Chemical reaction pathways of N_2O formation/consumption at flame zone (T = 1478 K) and at $\varphi = 1.4$ predicted by the Klippenstein kinetic model. Arrow lines refer to chemical transformations, percentages (%) refer to the contribution of reactants to the transformation, numbers stand for the net reaction rate in kmol/m^3s, which is also visualized by line thickness.

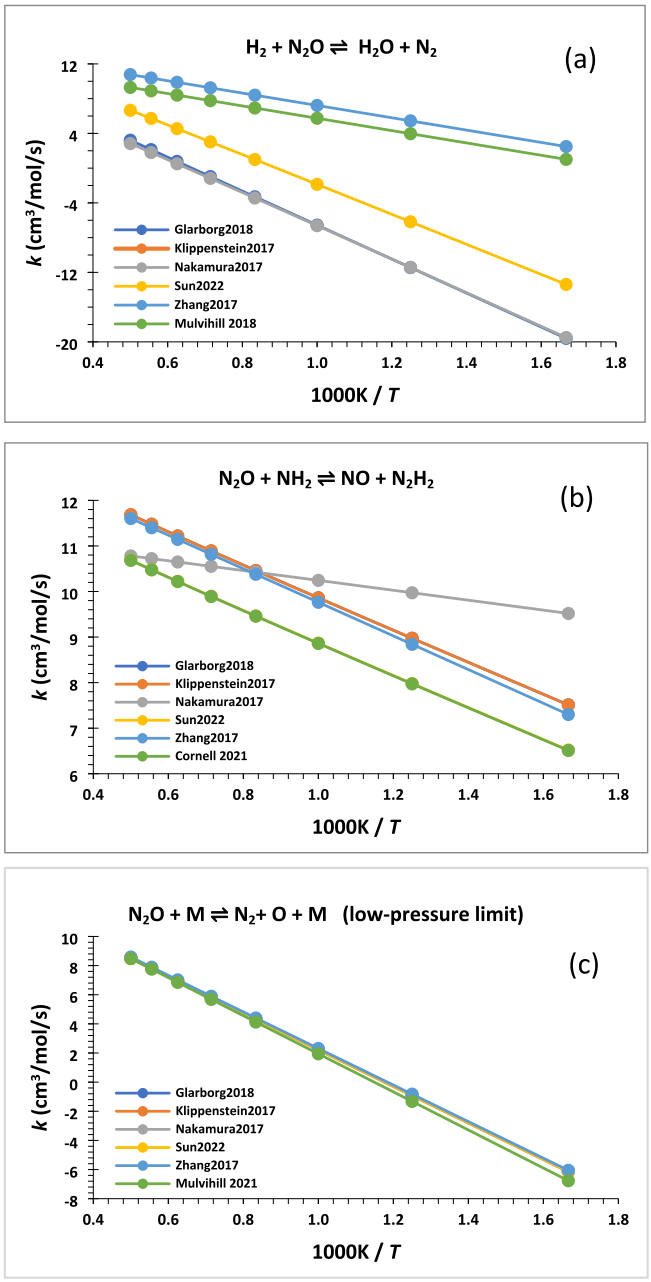

Fig. 31. Comparison of the rate constants for key reactions: (a) $H_2 + N_2O \rightleftharpoons H_2O + N_2$, (b) $N_2O + M \rightleftharpoons N_2 + O + M$ (low-pressure limit), and (c) $N_2O + NH_2 \rightleftharpoons NO + N_2H_2$, according to recent studies and the adopted values from the tested kinetic models.

On the other hand, the rate constant for the key reaction $N_2O + M \rightleftharpoons N_2 + O + M$, as shown Fig. 31 (c), is the same among the tested mechanisms. However, according to the study by Mulvihill et al. [89], the rate constant should be corrected when the temperature exceeds 1500 K for an accurate estimation of N_2O concentration due to the reaction's major role in determining the N_2O concentration under given conditions.

4. Conclusions

The present study numerically investigated the mole fraction of N_2O using 67 chemical kinetic mechanisms from the literature. The resulting numerical data were compared with experimental measurements from the literature using a normalised error approach, considering the uncertainty of the experimental measurements, to evaluate the performance of the selected mechanisms in predicting N_2O mole fractions in a 70/30 vol% NH_3/H_2 premixed flame. The study concludes that:

Based on the normalised error approach, most of the tested kinetic reaction mechanisms proved ineffective in predicting the N_2O mole fraction in the range of $\varphi = 0.57–0.65$, due to kinetic inhibition, which can lead to a failure to achieve ignition.
Klippenstein kinetic model generally predicts N_2O mole fractions accurately, but its performance deteriorates at very lean conditions ($\varphi = 0.57$).
The chemical reaction $NH + NO \rightleftharpoons N_2O + H$ significantly contributes to the formation of N_2O under all tested conditions. The reduction of N_2O is primarily controlled by the reactions $N_2O + H \rightleftharpoons N_2 + OH$, and $N_2O (+M) \rightleftharpoons N_2 + O(+M)$, which exhibit a dominant role across all equivalence ratios.
For local conditions of φ, the Nakamura mechanism shows good performance at 0.6, while the Zhang and Sun kinetic models demonstrate superior performance at stoichiometric and rich conditions, where the normalised errors of the aforementioned kinetic models were less than 1.

Lastly, this study's findings focused on 70/30 vol% NH_3/H_2 premixed flames at atmospheric conditions providing specific insights while also highlighting the limitations in assessing the generality of kinetic mechanisms. The majority of the evaluated models were developed for specific conditions, which limits their direct applicability to other NH_3/H_2 blends due to variations in N_2O sub-mechanisms. A more comprehensive evaluation of these mechanisms' generality and predictive accuracy would require a broader dataset covering various NH_3/H_2 blends and combustion systems. However, the current lack of such extensive experimental data, especially for the 70/30 vol% NH_3/H_2 blend, means that the broader applicability of these mechanisms in predicting N_2O mole fraction remains an open question. Therefore, the current study represents a significant step in understanding these mechanisms under specific conditions and underscores the need for further research to fully explore and validate their generality across diverse combustion environments.

CRediT authorship contribution statement

A. Alnasif: Writing – review & editing, Writing – original draft, Visualization, Validation, Software, Methodology, Investigation, Formal analysis, Data curation, Conceptualization. **J. Jójka:** Writing – review & editing, Validation, Software, Resources, Data curation. **S. Mashruk:** Writing – review & editing, Visualization, Resources, Data curation. **T. Nagy:** Writing – review & editing, Visualization, Validation, Data curation. **A. Valera-Medina:** Writing – review & editing, Visualization, Supervision, Resources, Project administration, Investigation, Funding acquisition.

Declaration of competing interest

The authors declare that they have no known competing financial interests or personal relationships that could have appeared to influence the work reported in this paper.

Data availability

Data will be made available on request.

Acknowledgments

The authors would like to express their gratitude for the support received from EPSRC through the SAFE-AGT Pilot project (No. EP/T009314/1), the Green Ammonia Thermal Propulsion MariNH3 project

(No. EP/W016656/1), and Project AMBURN with funding from the Department for Energy Security & Net Zero (DESNZ) under award (No. IFS2-06-FLO). Additionally, Joanna Jójka acknowledges the funding received for her doctoral fellowship from the National Science Centre, Poland, under grant (No. UMO-2019/32/T/ST8/00265). Ali Alnasif also extends his thanks to Al-Furat Al-Awsat Technical University (ATU) for financially supporting his PhD studies in the U.K. Furthermore, T. Nagy is thankful for the support provided by the FK134332 NKFIH grant.

Appendix A. Supplementary material

Supplementary data to this article can be found online at https://doi.org/10.1016/j.fuel.2024.131897.

References

[1] IEA (2021), Global Energy Review 2021. Paris: International Energy Agency, Https://Www.Iea.Org/Reports/Global-Energy-Review-2021 (n.d.).
[2] Astbury GR. A review of the properties and hazards of some alternative fuels. Process Saf Environ Prot 2008;86:397–414. https://doi.org/10.1016/J.PSEP.2008.05.001.
[3] Valera-Medina A, Xiao H, Owen-Jones M, David WIF, Bowen PJ. Ammonia for power. Prog Energy Combust Sci 2018;69:63–102. https://doi.org/10.1016/j.pecs.2018.07.001.
[4] Chai WS, Bao Y, Jin P, Tang G, Zhou L. A review on ammonia, ammonia-hydrogen and ammonia-methane fuels. Renew Sustain Energy Rev 2021;147. https://doi.org/10.1016/j.rser.2021.111254.
[5] Dimitriou P, Javaid R. A review of ammonia as a compression ignition engine fuel. Int J Hydrogen Energy 2020;45:7098–118. https://doi.org/10.1016/j.ijhydene.2019.12.209.
[6] Valera-Medina A, Amer-Hatem F, Azad AK, Dedoussi IC, De Joannon M, Fernandes RX, et al. Review on ammonia as a potential fuel: From synthesis to economics. Energy Fuel 2021;35:6964–7029. https://doi.org/10.1021/acs.energyfuels.0c03685.
[7] Crutzen PJ, Brauch HG. SPRINGER BRIEFS ON PIONEERS IN SCIENCE AND PRAC TICE NOBEL LAUREATES A Pioneer on Atmospheric Chemistry and Climate Change in the Anthropocene, n.d. http://www.afes-press-books.de/html/SpringerBriefs_PSP.htm.
[8] De Diego LF, Londonot CA, Wang XS, Gibbs BM. Influence of operating parameters on NOx and N20 axial profiles in a circulating fluidized bed combustor, 1996.
[9] Alnasif A, Mashruk S, Kovaleva M, Wang P, Valera-Medina A. Experimental and numerical analyses of nitrogen oxides formation in a high ammonia-low hydrogen blend using a tangential swirl burner. Carbon Neutrality 2022;1:24. https://doi.org/10.1007/s43979-022-00021-9.
[10] A. Hayakawa, M. Hayashi, G.J. Gotama, M. Kovaleva, E.C. Okafor, S. Colson, T. Kudo, S. Mashruk, A. Valera-Medina, H. Kobayashi, N2O Production Characteristics of Ammonia/Hydrogen/Air Premixed Laminar Flames Stabilized in Stagnation Flows at Lean Conditions, 2021.
[11] Mashruk S, Okafor EC, Kovaleva M, Alnasif A, Pugh D, Hayakawa A, et al. Evolution of N2O production at lean combustion condition in NH3/H2/air premixed swirling flames. Combust Flame 2022;244:112299. https://doi.org/10.1016/J.COMBUSTFLAME.2022.112299.
[12] Okafor EC, Tsukamoto M, Hayakawa A, Somarathne KDKA, Kudo T, Tsujimura T, et al. Influence of wall heat loss on the emission characteristics of premixed ammonia-air swirling flames interacting with the combustor wall. Proc Combust Inst 2021;38:5139–46. https://doi.org/10.1016/j.proci.2020.06.142.
[13] Gotama GJ, Hayakawa A, Okafor EC, Kanoshima R, Hayashi M, Kudo T, et al. Measurement of the laminar burning velocity and kinetics study of the importance of the hydrogen recovery mechanism of ammonia/hydrogen/air premixed flames. Combust Flame 2022;236. https://doi.org/10.1016/j.combustflame.2021.111753.
[14] Nakamura H, Hasegawa S, Tezuka T. Kinetic modeling of ammonia/air weak flames in a micro flow reactor with a controlled temperature profile. Combust Flame 2017;185:16–27. https://doi.org/10.1016/j.combustflame.2017.06.021.
[15] Glarborg P. The NH3/NO2/O2 system: Constraining key steps in ammonia ignition and N2O formation. Combust Flame 2022. https://doi.org/10.1016/j.combustflame.2022.112311.
[16] Stagni A, Cavallotti C, Arunthanayothin S, Song Y, Herbinet O, Battin-Leclerc F, et al. An experimental, theoretical and kinetic-modeling study of the gas-phase oxidation of ammonia. React Chem Eng 2020;5:696–711. https://doi.org/10.1039/c9re00429g.
[17] Mørch CS, Bjerre A, Gøttrup MP, Sorenson SC, Schramm J. Ammonia/hydrogen mixtures in an SI-engine: Engine performance and analysis of a proposed fuel system. Fuel 2011;90:854–64. https://doi.org/10.1016/j.fuel.2010.09.042.
[18] Zhang X, Moosakutty SP, Rajan RP, Younes M, Sarathy SM. Combustion chemistry of ammonia/hydrogen mixtures: Jet-stirred reactor measurements and comprehensive kinetic modeling. Combust Flame 2021;234. https://doi.org/10.1016/j.combustflame.2021.111653.
[19] Hayakawa A, Hayashi M, Kovaleva M, Gotama GJ, Okafor EC, Colson S, et al., Experimental and numerical study of product gas and N2O emission characteristics of ammonia/hydrogen/air premixed laminar flames stabilized in a stagnation flow, Proceedings of the Combustion Institute (2022). doi: 10.1016/j.proci.2022.08.124.
[20] Brackmann C, Alekseev VA, Zhou B, Nordström E, Bengtsson P-E, Li Z, et al. Structure of premixed ammonia + air flames at atmospheric pressure: Laser diagnostics and kinetic modeling. Combust Flame 2016;163:370–81. https://doi.org/10.1016/j.combustflame.2015.10.012.
[21] CHEMKIN-Pro, version 19.2, ANSYS, (2019).
[22] Hayakawa A, Hirano Y, Okafor EC, Yamashita H, Kudo T, Kobayashi H. Experimental and numerical study of product gas characteristics of ammonia/air premixed laminar flames stabilized in a stagnation flow. Proc Combust Inst 2021;38:2409–17. https://doi.org/10.1016/j.proci.2020.07.030.
[23] Bertolino A, Fürst M, Stagni A, Frassoldati A, Pelucchi M, Cavallotti C, et al. An evolutionary, data-driven approach for mechanism optimization: theory and application to ammonia combustion. Combust Flame 2021;229. https://doi.org/10.1016/j.combustflame.2021.02.012.
[24] Dagaut P, Glarborg P, Alzueta MU. The oxidation of hydrogen cyanide and related chemistry. Prog Energy Combust Sci 2008;34:1–46. https://doi.org/10.1016/j.pecs.2007.02.004.
[25] Mei B, Ma S, Zhang X, Li Y. Characterizing ammonia and nitric oxide interaction with outwardly propagating spherical flame method, Proceedings of the Combustion Institute 38 (2021) 2477–2485. doi: 10.1016/j.proci.2020.07.133.
[26] Smith Gregory P, Golden David M, Michael Frenklach, Moriarty Nigel W, Boris Eiteneer, Mikhail Goldenberg, Thomas Bowman C, Ronald K. Hanson, Soonho Song, William C. Gardiner, V.V.L. Jr., Zhiwei Qin, GRI-Mech 3.0, Http://Www.Me.Berkeley.Edu/Gri_mech/ (2000).
[27] Han X, Marco LL, Brackmann C, Wang Z, He Y, Konnov AA. Experimental and kinetic modeling study of NO formation in premixed CH4+O2+N2 flames. Combust Flame 2021;223:349–60. https://doi.org/10.1016/j.combustflame.2020.10.010.
[28] Coda Zabetta E, Hupa M. A detailed kinetic mechanism including methanol and nitrogen pollutants relevant to the gas-phase combustion and pyrolysis of biomass-derived fuels. Combust Flame 2008;152:14–27. https://doi.org/10.1016/j.combustflame.2007.06.022.
[29] Tang R, Xu Q, Pan J, Gao J, Wang Z, Wei H, et al. An experimental and modeling study of ammonia oxidation in a jet stirred reactor. Combust Flame 2022;240. https://doi.org/10.1016/j.combustflame.2022.112007.
[30] Alzueta MU, Zaragoza-2016 Mechanism , Personal Communication (2016).
[31] Shmakov AG, Korobeinichev OP, Rybitskaya IV, Chernov AA, Knyazkov DA, Bolshova TA, et al. Formation and consumption of NO in H2 + O2 + N2 flames doped with NO or NH3 at atmospheric pressure. Combust Flame 2010;157:556–65. https://doi.org/10.1016/j.combustflame.2009.10.008.
[32] Shrestha KP, Lhuillier C, Barbosa AA, Brequigny P, Contino F, Mounaïm-Rousselle C, et al. An experimental and modeling study of ammonia with enriched oxygen content and ammonia/hydrogen laminar flame speed at elevated pressure and temperature. Proc Combust Inst 2021;38:2163–74. https://doi.org/10.1016/j.proci.2020.06.197.
[33] Esarte C, Peg M, Ruiz MP, Millera Á, Bilbao R, Alzueta MU. Pyrolysis of ethanol: Gas and soot products formed. Ind Eng Chem Res 2011;50:4412–9. https://doi.org/10.1021/ie1022628.
[34] Wang Z, Han X, He Y, Zhu R, Zhu Y, Zhou Z, et al. Experimental and kinetic study on the laminar burning velocities of NH3 mixing with CH3OH and C2H5OH in premixed flames. Combust Flame 2021;229. https://doi.org/10.1016/j.combustflame.2021.02.038.
[35] Abian M, Alzueta MU, Glarborg P. Formation of NO from N2/O2 mixtures in a flow reactor: Toward an accurate prediction of thermal NO. Int J Chem Kinet 2015;47:518–32. https://doi.org/10.1002/kin.20929.
[36] Wang T, Zhang X, Zhang J, Hou X. Automatic generation of a kinetic skeletal mechanism for methane-hydrogen blends with nitrogen chemistry. Int J Hydrogen Energy 2018;43:3330–41. https://doi.org/10.1016/j.ijhydene.2017.12.116.
[37] Arunthanayothin S, Stagni A, Song Y, Herbinet O, Faravelli T, Battin-Leclerc F. Ammonia-methane interaction in jet-stirred and flow reactors: An experimental and kinetic modeling study, in: Proceedings of the Combustion Institute, Elsevier Ltd, 2021: pp. 345–353. doi: 10.1016/j.proci.2020.07.061.
[38] Faravelli T. POLIMI-2017, Personal Communication (2017).
[39] POLIMI, The CRECK Modeling Group,C1-C3 mechanism , Http://Creckmodeling.Chem.Polimi.It. (2014).
[40] Han X, Wang Z, Costa M, Sun Z, He Y, Cen K. Experimental and kinetic modeling study of laminar burning velocities of NH3/air, NH3/H2/air, NH3/CO/air and NH3/CH4/air premixed flames. Combust Flame 2019;206:214–26. https://doi.org/10.1016/j.combustflame.2019.05.003.
[41] Marques CST, Dos Santos LR, Sbampato ME, Barreta LG, Dos Santos AM. TEMPERATURE MEASUREMENTS BY OH LIF AND CHEMILUMINESCENCE KINETIC MODELING FOR ETHANOL FLAMES, 2073.
[42] de Persis S, Pillier L, Idir M, Molet J, Lamoureux N, Desgroux P. NO formation in high pressure premixed flames: Experimental results and validation of a new revised reaction mechanism. Fuel 2020;260. https://doi.org/10.1016/j.fuel.2019.116331.
[43] Aranda V, Christensen JM, Alzueta MU, Glarborg P, Gersen S, Gao Y, et al. Experimental and kinetic modeling study of methanol ignition and oxidation at high pressure. Int J Chem Kinet 2013;45:283–94. https://doi.org/10.1002/kin.20764.
[44] Mei B, Zhang X, Ma S, Cui M, Guo H, Cao Z, et al. Experimental and kinetic modeling investigation on the laminar flame propagation of ammonia under oxygen enrichment and elevated pressure conditions. Combust Flame 2019;210:236–46. https://doi.org/10.1016/j.combustflame.2019.08.033.
[45] Jiang Y, Gruber A, Seshadri K, Williams F. An updated short chemical-kinetic nitrogen mechanism for carbon-free combustion applications. Int J Energy Res 2020;44:795–810. https://doi.org/10.1002/er.4891.

[46] Li R, Konnov AA, He G, Qin F, Zhang D. Chemical mechanism development and reduction for combustion of NH3/H2/CH4 mixtures. Fuel 2019;257. https://doi.org/10.1016/j.fuel.2019.116059.

[47] Sun J, Yang Q, Zhao N, Chen M, Zheng H. Numerically study of CH4/NH3 combustion characteristics in an industrial gas turbine combustor based on a reduced mechanism. Fuel 2022;327:124897. https://doi.org/10.1016/J.FUEL.2022.124897.

[48] Okafor EC, Naito Y, Colson S, Ichikawa A, Kudo T, Hayakawa A, et al. Measurement and modelling of the laminar burning velocity of methane-ammonia-air flames at high pressures using a reduced reaction mechanism. Combust Flame 2019;204:162–75. https://doi.org/10.1016/j.combustflame.2019.03.008.

[49] Song Y, Marrodán L, Vin N, Herbinet O, Assaf E, Fittschen C, et al. The sensitizing effects of NO 2 and NO on methane low temperature oxidation in a jet stirred reactor. Proc Combust Inst 2019;37:667–75. https://doi.org/10.1016/j.proci.2018.06.115.

[50] Glarborg P, Miller JA, Ruscic B, Klippenstein SJ. Modeling nitrogen chemistry in combustion. Prog Energy Combust Sci 2018;67:31–68. https://doi.org/10.1016/j.pecs.2018.01.002.

[51] Mével R, Javoy S, Lafosse F, Chaumeix N, Dupré G, Paillard CE. Hydrogen–nitrous oxide delay times: Shock tube experimental study and kinetic modelling. Proc Combust Inst 2009;32:359–66. https://doi.org/10.1016/J.PROCI.2008.06.171.

[52] Shrestha KP, Seidel L, Zeuch T, Mauss F. Detailed Kinetic Mechanism for the Oxidation of Ammonia Including the Formation and Reduction of Nitrogen Oxides. Energy Fuel 2018;32:10202–17. https://doi.org/10.1021/acs.energyfuels.8b01056.

[53] da Rocha RC, Costa M, Bai XS. Chemical kinetic modelling of ammonia/hydrogen/air ignition, premixed flame propagation and NO emission. Fuel 2019;246:24–33. https://doi.org/10.1016/J.FUEL.2019.02.102.

[54] Otomo J, Koshi M, Mitsumori T, Iwasaki H, Yamada K. Chemical kinetic modeling of ammonia oxidation with improved reaction mechanism for ammonia/air and ammonia/hydrogen/air combustion. Int J Hydrogen Energy 2018;43:3004–14. https://doi.org/10.1016/j.ijhydene.2017.12.066.

[55] U. Mechanism, Chemical-kinetic mechanisms for combustion applications, Mechanical and Aerospace Engineering (Combustion Research), University of California at San Diego (2018).

[56] Klippenstein SJ, Pfeifle M, Jasper AW, Glarborg P. Theory and modeling of relevance to prompt-NO formation at high pressure. Combust Flame 2018;195:3–17. https://doi.org/10.1016/j.combustflame.2018.04.029.

[57] Kovaleva M, Hayakawa A, Colson S, Okafor EC, Kudo T, Valera-Medina A, et al. Numerical and experimental study of product gas characteristics in premixed ammonia/methane/air laminar flames stabilised in a stagnation flow. Fuel Communications 2022;10:100054. https://doi.org/10.1016/j.jfueco.2022.100054.

[58] Houshfar E, Skreiberg Ø, Glarborg P, Løvas T. Reduced chemical kinetic mechanisms for NO x emission prediction in biomass combustion. Int J Chem Kinet 2012;44:219–31. https://doi.org/10.1002/kin.20716.

[59] Zhang Y, Mathieu O, Petersen EL, Bourque G, Curran HJ. Assessing the predictions of a NOx kinetic mechanism on recent hydrogen and syngas experimental data. Combust Flame 2017;182:122–41. https://doi.org/10.1016/j.combustflame.2017.03.019.

[60] Lamoureux N, El Merhubi H, Pillier L, de Persis S, Desgroux P. Modeling of NO formation in low pressure premixed flames. Combust Flame 2016;163:557–75. https://doi.org/10.1016/j.combustflame.2015.11.007.

[61] Xiao H, Valera-Medina A, Bowen PJ. Modeling Combustion of Ammonia/Hydrogen Fuel Blends under Gas Turbine Conditions. Energy Fuel 2017;31:8631–42. https://doi.org/10.1021/acs.energyfuels.7b00709.

[62] Capriolo G, Brackmann C, Lubrano Lavadera M, Methling T, Konnov AA. An experimental and kinetic modeling study on nitric oxide formation in premixed C3alcohols flames. In: Proceedings of the Combustion Institute, Elsevier Ltd, 2021: pp. 805–812. doi: 10.1016/j.proci.2020.07.051.

[63] Song Y, Hashemi H, Christensen JM, Zou C, Marshall P, Glarborg P. Ammonia oxidation at high pressure and intermediate temperatures. Fuel 2016;181:358–65. https://doi.org/10.1016/j.fuel.2016.04.100.

[64] Xu L, Chang Y, Treacy M, Zhou Y, Jia M, Bai XS. A skeletal chemical kinetic mechanism for ammonia/n-heptane combustion. Fuel 2023;331. https://doi.org/10.1016/j.fuel.2022.125830.

[65] Nozari H, Karabeyoğlu A. Numerical study of combustion characteristics of ammonia as a renewable fuel and establishment of reduced reaction mechanisms. Fuel 2015;159:223–33. https://doi.org/10.1016/j.fuel.2015.06.075.

[66] Thomas DE, Shrestha KP, Mauss F, Northrop WF. ARTICLE IN PRESS Extinction and NO formation of ammonia-hydrogen and air non-premixed counterflow flames. Proc Combust Inst 2022. https://doi.org/10.1016/j.proci.2022.08.067.

[67] Mathieu O, Petersen EL. Experimental and modeling study on the high-temperature oxidation of Ammonia and related NOx chemistry. Combust Flame 2015;162:554–70. https://doi.org/10.1016/j.combustflame.2014.08.022.

[68] Kovács M, Papp M, Zsély IG, Turányi T. Determination of rate parameters of key N/H/O elementary reactions based on H2/O2/NOx combustion experiments. Fuel 2020;264:116720. https://doi.org/10.1016/J.FUEL.2019.116720.

[69] Duynslaegher C, Contino F, Vandooren J, Jeanmart H. Modeling of ammonia combustion at low pressure. Combust Flame 2012;159:2799–805. https://doi.org/10.1016/j.combustflame.2012.06.003.

[70] M. Kovács Máté Papp István Gy Zsély Tamás Turányi, Main sources of uncertainty in recent methanol/NOx combustion models, Int J Chem Kinet 53 (2021) 884–900. doi: 10.1002/kin.21490.

[71] Klippenstein SJ, Harding LB, Glarborg P, Miller JA. The role of NNH in NO formation and control. Combust Flame 2011;158:774–89. https://doi.org/10.1016/j.combustflame.2010.12.013.

[72] Saxena P, Williams FA. Numerical and experimental studies of ethanol flames. In: Proceedings of the Combustion Institute 31 I; 2007. p. 1149–56. https://doi.org/10.1016/j.proci.2006.08.097.

[73] Zhang K, Li Y, Yuan T, Cai J, Glarborg P, Qi F. An experimental and kinetic modeling study of premixed nitromethane flames at low pressure. Proc Combust Inst 2011;33:407–14. https://doi.org/10.1016/j.proci.2010.06.002.

[74] Valkó É, Papp M, Kovács M, Varga T, Gy Zsély I, Nagy T, et al. Combustion Theory and Modelling ISSN: (Print) (Design of combustion experiments using differential entropy Design of combustion experiments using differential entropy. Combust Theor Model 2022;26:67–90. https://doi.org/10.1080/13647830.2021.1992506.

[75] Lamoureux N, Desgroux P, El Bakali A, Pauwels JF. Experimental and numerical study of the role of NCN in prompt-NO formation in low-pressure CH4-O2-N2 and C2H2-O2-N2 flames. Combust Flame 2010;157:1929–41. https://doi.org/10.1016/j.combustflame.2010.03.013.

[76] Alzueta MU, Bilbao R, Finestra M. Methanol oxidation and its interaction with nitric oxide. Energy Fuel 2001;15:724–9. https://doi.org/10.1021/ef0002602.

[77] Konnov AA. Implementation of the NCN pathway of prompt-NO formation in the detailed reaction mechanism. Combust Flame 2009;156:2093–105. https://doi.org/10.1016/j.combustflame.2009.03.016.

[78] Nakamura H, Shindo M. Effects of radiation heat loss on laminar premixed ammonia/air flames. Proc Combust Inst 2019;37:1741–8. https://doi.org/10.1016/j.proci.2018.06.138.

[79] Mendiara T, Glarborg P. Ammonia chemistry in oxy-fuel combustion of methane. Combust Flame 2009;156:1937–49. https://doi.org/10.1016/j.combustflame.2009.07.006.

[80] Tian Z, Li Y, Zhang L, Glarborg P, Qi F. An experimental and kinetic modeling study of premixed NH3/CH4/O2/Ar flames at low pressure. Combust Flame 2009;156:1413–26. https://doi.org/10.1016/j.combustflame.2009.03.005.

[81] Nagy T *, Turányi T. Minimal Spline Fit: a model-free method for determining statistical noise of experimental data series, n.d.

[82] Klippenstein SJ, Glarborg P. Theoretical kinetics predictions for NH2 + HO2. Combust Flame 2022;236:111787. https://doi.org/10.1016/j.combustflame.2021.111787.

[83] Dai L, Gersen S, Glarborg P, Levinsky H, Mokhov A. Experimental and numerical analysis of the autoignition behavior of NH3 and NH3/H2 mixtures at high pressure. Combust Flame 2020;215:134–44. https://doi.org/10.1016/j.combustflame.2020.01.023.

[84] Dai L, Hashemi H, Glarborg P, Gersen S, Marshall P, Mokhov A, et al. Ignition delay times of NH3 /DME blends at high pressure and low DME fraction: RCM experiments and simulations. Combust Flame 2021;227:120–34. https://doi.org/10.1016/j.combustflame.2020.12.048.

[85] Stagni A, Cavallotti C. H-abstractions by O2, NO2, NH2, and HO2 from H2NO: Theoretical study and implications for ammonia low-temperature kinetics. Proc Combust Inst 2022. https://doi.org/10.1016/j.proci.2022.08.024.

[86] Alnasif A, Zitouni S, Mashruk S, Brequigny P, Kovaleva M, Mounaim-rousselle C, et al. Experimental and numerical comparison of currently available reaction mechanisms for laminar flame speed in 70/30 (%vol.) NH3/H2 flames, Applications in Energy and Combustion. Science 2023;14. https://doi.org/10.1016/j.jaecs.2023.100139.

[87] Cornell RE, Barbet MC, Burke MP. Toward a more comprehensive understanding of the kinetics of a common biomass-derived impurity: NH3 oxidation by N2O in a jet-stirred reactor. Energy Fuel 2021;35:13338–48. https://doi.org/10.1021/acs.energyfuels.1c01544.

[88] Mulvihill CR, Mathieu O, Petersen EL. The unimportance of the reaction H2 + N2O ⇆ H2O + N2: A shock-tube study using H2O time histories and ignition delay times. Combust Flame 2018;196:478–86. https://doi.org/10.1016/j.combustflame.2018.07.003.

[89] Mulvihill CR, Alturaifi SA, Petersen EL. A shock-tube study of the N2O + M ⇄ N2 + O + M (M = Ar) rate constant using N2O laser absorption near 4.6 μm. Combust Flame 224 2021:6–13. https://doi.org/10.1016/j.combustflame.2020.10.040.